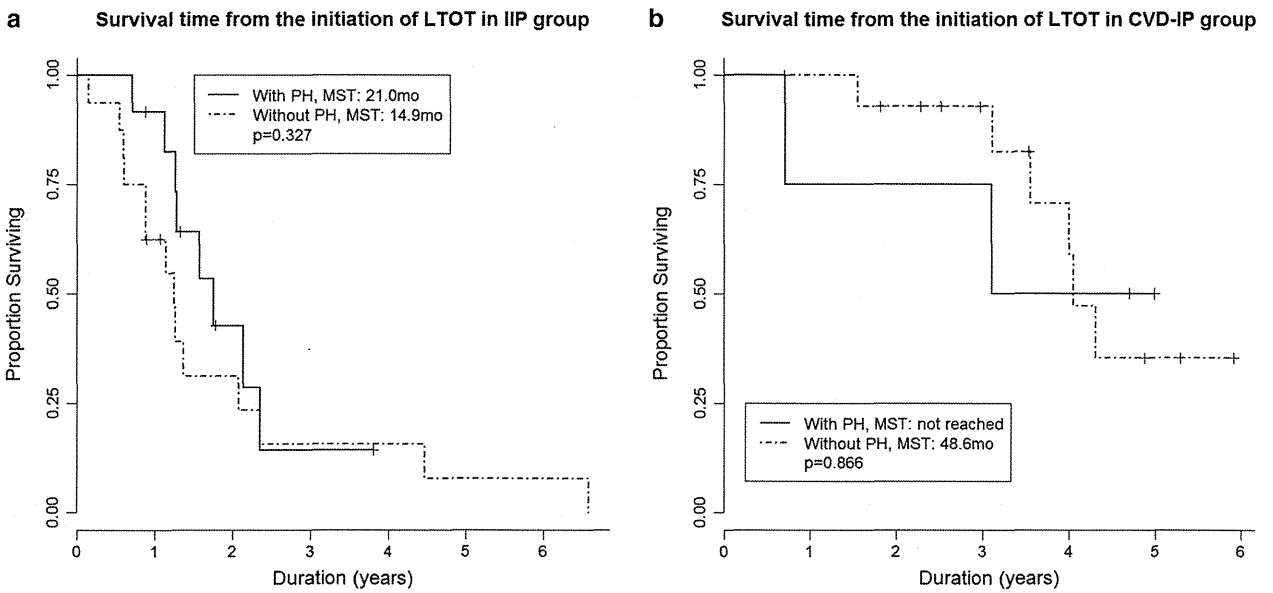

Fig. 4 a Survival curves for IIP patients with pulmonary hypertension (PH) ($n = 12$) and those without PH ($n = 16$). Survival time did not differ significantly between the groups ($p = 0.327$). **b** Survival curves for patients with CVD-IP patient with PH ($n = 4$) and those without PH ($n = 15$). Survival time did not differ significantly between the groups ($p = 0.866$)

Table 4 Results of univariate Cox analysis

	HR	95 % CI	*p* value
Age per 5 years	1.28	1.11–1.47	0.001*
Female gender	0.50	0.28–0.89	0.017*
BMI per 5	0.67	0.44–1.05	0.082
UIP	1.87	1.05–3.33	0.033*
Presence of honeycombing	1.76	0.89–3.46	0.101
Presence of CVD	0.20	0.10–0.41	<0.001*
FVC per 5 % predicted	1.02	0.93–1.12	0.635
FEV_1 per 5 % predicted	1.04	0.95–1.14	0.336
DL_{CO} per 5 % predicted	0.99	0.89–1.12	0.982
PaO_2 per 5 mmHg	0.98	0.87–1.09	0.740
$PaCO_2$ per 5 mmHg	1.44	1.10–1.88	0.007*
KL-6 per 100 U/ml	0.99	0.96–1.02	0.516

HR hazard ratio, *CI* confidence interval, *BMI* body mass index, *UIP* usual interstitial pneumonia, *CVD* collagen vascular disease, *FVC* forced vital capacity, FEV_1 forced expiratory volume in 1 s, DL_{CO} carbon monoxide diffusing capacity, PaO_2 partial oxygen pressure in the arterial blood gas, $PaCO_2$ partial carbon dioxide pressure in the arterial blood gas, *KL-6* Krebs von den Lungen-6

* Statistical significance

Table 5 Results of multivariate Cox analysis

	HR	95 % CI	*p* value
Age per 5 years	1.13	0.96–1.33	0.119
Female gender	0.48	0.24–0.95	0.036*
BMI per 5	0.43	0.24–0.76	0.003*
UIP	0.93	0.43–2.03	0.874
Presence of CVD	0.17	0.07–0.43	<0.001*
$PaCO_2$ per 5 mmHg	1.20	0.88–1.64	0.236

HR hazard ratio, *CI* confidence interval, *BMI* body mass index, *UIP* usual interstitial pneumonia, *CVD* collagen vascular disease, $PaCO_2$ partial carbon dioxide pressure in the arterial blood gas

* Statistical significance

survival rates of 77.6 and 88.9 %, respectively, and 5-year survival rates of 67.4 and 81.5 %, respectively (p = 0.2). These results suggest that CVD-UIP has a better survival than IPF (IPF-UIP), which is consistent with the results of Song et al. [8]. Taken together, these results indicate that the presence of CVD is associated with a better prognosis in patients with UIP histology, but not in those with NSIP histology. However, the survival times measured in most studies might have been unreliable because the timing of the IP diagnosis is usually obscure. For instance, CVD-IP is often diagnosed while the underlying CVD is being followed; therefore, the survival time could be accordingly overestimated. Our study suggested that CVD-IP is still associated with a better prognosis than IIP even after these diseases have worsened to an oxygen-dependent state.

Although surgical lung biopsy is regarded as the most reliable method for classifying disease phenotypes, we often prefer to use HRCT findings for making classification decisions because of the risks associated with the surgical procedure, especially in patients with severe disease. The association between HRCT findings and prognosis is clinically important, and HRCT classifications have been

evaluated against histologic findings in several studies. In a report by Flaherty et al. [20], the HRCT images in 73 patients who had IIP with histologically proven UIP patterns (IIP-UIP) were classified as definite UIP, probable UIP, intermediate, probable NSIP, and definite NSIP patterns. The patients with HRCT patterns interpreted as definite UIP or probable UIP had significantly shorter survival times compared to those with other HRCT patterns. Therefore, this study suggests that HRCT patterns can be associated with prognosis even in patients with UIP on histology. However, Sumikawa et al. [21] reported conflicting results. These authors categorized the HRCT images of patients with histologically proven IPF as definite UIP, consistent with UIP, and suggestive of an alternative diagnosis, but they did not find any significant difference in survival among the 3 HRCT patterns. We failed to find differences in survival between the HRCT patterns based on the 2011 ATS/ERS statement and between the presence and absence of honeycombing in our cohort. Although histological examinations were performed for few patients in our study, we propose 2 possible explanations for the results regarding the HRCT patterns. First, many of the patients with a HRCT pattern inconsistent with UIP might have had histologic UIP. Second, the prognosis might have been poor even for patients with histology other than UIP once they became oxygen-dependent.

In our study, acute exacerbation was the most frequent cause of death for patients with IIP, while it was rare in those with CVD-IP. Acute exacerbation is a devastating event and is an important cause of death, especially in IPF. Daniels et al., who reviewed autopsy reports from 42 patients with IPF, reported that respiratory-related causes accounted for 64 % of deaths; among these respiratory-related causes, acute exacerbation occurred with the highest frequency, followed by pneumonia and gradual progression of disease [22]. Although acute exacerbation is known to occur in patients with CVD-IP, it occurs at a lower frequency in CVD-IP patients compared to in patients with IPF [23]; this may partly account for the better prognosis of CVD-IP observed in our cohort.

In our study, male gender, low BMI, and the absence of CVD were independently associated with a poor prognosis after adjusting for confounders. We excluded the factor of the presence of honeycombing from the multivariate analysis although the p value of the factor in the univariate analysis was almost near 0.1. Otherwise, including both factors of UIP pattern and the presence of honeycombing can cause a problem of multicollinearity because there was a strong correlation between these two factors ($p < 0.001$ on Fisher's exact test). Even when the presence of honeycombing was included in the multivariate analysis, the results did not change significantly (data not shown). Previous studies have also reported that gender and BMI are significant prognostic factors [24, 25]. Conversely, Kondoh et al. [26] who retrospectively analyzed 110 patients with IPF, showed that high BMI was an independent risk factor for acute exacerbation of IPF (hazard ratio, 1.20; 95 % confidence interval, 1.46–5.85; $p < 0.001$), but it was not associated with survival (hazard ratio, 0.97; 95 % confidence interval, 0.88–1.07; $p = 0.590$) [26]. Pulmonary function data, particularly carbon monoxide diffusing capacity (DL_{CO}) <40 % of predicted value, are also reported to be useful prognostic indicators [2, 18]. However, no correlation between spirometric data and prognosis was found in our study, possibly due to patient selection. Our study included patients receiving LTOT, and more than 85 % of these patients had severely impaired pulmonary function, with DL_{CO} <40 % of predicted value. Thus, the usefulness of a pulmonary function test as an independent predictor of survival was likely negated in this population.

PH is a common condition and has been demonstrated to be an important poor prognostic factor in IPF [27] and systemic sclerosis [28]. However, the association between PH and survival was unclear in this study. This may be because few patients underwent evaluation for pulmonary hemodynamics, and most patients were evaluated with UCG. UCG is often performed to evaluate pulmonary hemodynamics as a substitutive method for right heart catheterization because it is less invasive and less time consuming. However, UCG is a less reliable measure than catheterization for detecting PH [19].

This study had several limitations. First, this was a single-center retrospective study consisting of a small sample size. Second, histologic examinations were not performed in the majority of the patients. Finally, the association between treatments other than LTOT and the prognosis was not examined because evaluating treatment effects in a study with a retrospective design would be difficult and would yield potentially misleading results. However, even with these limitations, our study provides clinically useful information regarding the prognosis from the initiation of LTOT and the prognostic factors in this clinical setting because the data reflect real clinical practice.

Conclusions

The present study showed that the prognosis of oxygen-dependent IP is poor, especially in patients with IIP, regardless of the HRCT pattern. Male gender, low BMI, and the absence of CVD were the independent negative prognostic factors in patients with IP receiving LTOT. It is

important that we continue to advance our understanding of the pathogenesis of IPs and develop novel treatments.

Conflict of interest None.

References

1. Travis WD, Costabel U, Hansell DM, King TE Jr, Lynch DA, Nicholson AG, Ryerson CJ, Ryu JH, Selman M, Wells AU, Behr J, Bouros D, Brown KK, Colby TV, Collard HR, Cordeiro CR, Cottin V, Crestani B, Drent M, Dudden RF, Egan J, Flaherty K, Hogaboam C, Inoue Y, Johkoh T, Kim DS, Kitaichi M, Loyd J, Martinez FJ, Myers J, Protzko S, Raghu G, Richeldi L, Sverzellati N, Swigris J, Valeyre D; ATS/ERS Committee on Idiopathic Interstitial Pneumonias (2013) An official American Thoracic Society/European Respiratory Society statement: update of the international multidisciplinary classification of the idiopathic interstitial pneumonias. Am J Respir Crit Care Med 188:733–748
2. Raghu G, Collard HR, Egan JJ, Martinez FJ, Behr J, Brown KK, Colby TV, Cordier JF, Flaherty KR, Lasky JA, Lynch DA, Ryu JH, Swigris JJ, Wells AU, Ancochea J, Bouros D, Carvalho C, Costabel U, Ebina M, Hansell DM, Johkoh T, Kim DS, King TE Jr, Kondoh Y, Myers J, Müller NL, Nicholson AG, Richeldi L, Selman M, Dudden RF, Griss BS, Protzko SL, Schünemann HJ; ATS/ERS/JRS/ALAT Committee on Idiopathic Pulmonary Fibrosis (2011) An official ATS/ERS/JRS/ALAT statement: idiopathic pulmonary fibrosis: evidence-based guidelines for diagnosis and management. Am J Respir Crit Care Med 183:788–824
3. King TE Jr, Pardo A, Selman M (2011) Idiopathic pulmonary fibrosis. Lancet 378:1949–1961
4. Tansey D, Wells AU, Colby TV, Ip S, Nikolakoupolou A, du Bois RM, Hansell DM, Nicholson AG (2004) Variations in histological patterns of interstitial pneumonia between connective tissue disorders and their relationship to prognosis. Histopathology 44:585–596
5. Cottin V (2013) Significance of connective tissue diseases features in pulmonary fibrosis. Eur Respir Rev 22:273–280
6. Bradley B, Branley HM, Egan JJ, Greaves MS, Hansell DM, Harrison NK, Hirani N, Hubbard R, Lake F, Millar AB, Wallace WA, Wells AU, Whyte MK, Wilsher ML; British Thoracic Society Interstitial Lung Disease Guideline Group, British Thoracic Society Standards of Care Committee; Thoracic Society of Australia; New Zealand Thoracic Society; Irish Thoracic Society (2008) Interstitial lung disease guideline: the British Thoracic Society in collaboration with the Thoracic Society of Australia and New Zealand and the Irish Thoracic Society. Thorax 63:v1–v58
7. Park JH, Kim DS, Park IN, Jang SJ, Kitaichi M, Nicholson AG, Colby TV (2007) Prognosis of fibrotic interstitial pneumonia: idiopathic versus collagen vascular disease-related subtypes. Am J Respir Crit Care Med 175:705–711
8. Song JW, Do KH, Kim MY, Jang SJ, Colby TV, Kim DS (2009) Pathologic and radiologic differences between idiopathic and collagen vascular disease-related usual interstitial pneumonia. Chest 136:23–30
9. Travis WD, Matsui K, Moss J, Ferrans VJ (2000) Idiopathic nonspecific interstitial pneumonia: prognostic significance of cellular and fibrosing patterns: survival comparison with usual interstitial pneumonia and desquamative interstitial pneumonia. Am J Surg Pathol 24:19–33
10. Nicholson AG, Colby TV, du Bois RM, Hansell DM, Wells AU (2000) The prognostic significance of the histologic pattern of interstitial pneumonia in patients presenting with the clinical entity of cryptogenic fibrosing alveolitis. Am J Respir Crit Care Med 162:2213–2217
11. Arnett FC, Edworthy SM, Bloch DA, Mcshane DJ, Fries JF, Cooper NS, Healey LA, Kaplan SR, Liang MH, Luthra HS, Medsger TA Jr, Mitchell DM, Neustadt DH, Pinals RS, Schaller JG, Sharp JT, Wilder RL, Hunder GG (1988) The American Rheumatism Association 1987 revised criteria for the classification of rheumatoid arthritis. Arthritis Rheum 31:315–324
12. Dr. Alfonse T. Masi, Subcommittee For Scleroderma Criteria of the American Rheumatism Association Diagnostic and Therapeutic Criteria Committee (1980) Preliminary criteria for the classification of systemic sclerosis (scleroderma). Subcommittee for scleroderma criteria of the American Rheumatism Association Diagnostic and Therapeutic Criteria Committee. Arthritis Rheum 23:581–590
13. Smolen JS, Steiner G (1998) Mixed connective tissue disease: to be or not to be? Arthritis Rheum 41:768–777
14. Bohan A, Peter JB (1975) Polymyositis and dermatomyositis (first of two parts). N Engl J Med 292:344–347
15. Vitali C, Bombardieri S, Jonsson R, Moutsopoulos HM, Alexander EL, Carsons SE, Daniels TE, Fox PC, Fox RI, Kassan SS, Pillemer SR, Talal N, Weisman MH, European Study Group on Classification Criteria for Sjögren's Syndrome (2002) Classification criteria for Sjogren's syndrome: a revised version of the European criteria proposed by the American-European Consensus Group. Ann Rheum Dis 61:554–558
16. Akira M, Hamada H, Sakatani M, Kobayashi C, Nishioka M, Yamamoto S (1997) CT findings during phase of accelerated deterioration in patients with idiopathic pulmonary fibrosis. Am J Roentgenol 168:79–83
17. R Core Team (2013) R: A language and environment for statistical computing. R Foundation for Statistical Computing, Vienna, Austria. http://www.R-project.org/
18. Badesch DB, Champion HC, Sanchez MA, Hoeper MM, Loyd JE, Manes A, McGoon M, Naeije R, Olschewski H, Oudiz RJ, Torbicki A (2009) Diagnosis and assessment of pulmonary arterial hypertension. J Am Coll Cardiol 54:S55–S66
19. Mura M, Porretta MA, Bargagli E, Sergiacomi G, Zompatori M, Sverzellati N, Taglieri A, Mezzasalma F, Rottoli P, Saltini C, Rogliani P (2012) Predicting survival in newly diagnosed idiopathic pulmonary fibrosis: a 3-year prospective study. Eur Respir J 40:101–109
20. Flaherty KR, Thwaite EL, Kazerooni EA, Gross BH, Toews GB, Colby TV, Travis WD, Mumford JA, Murray S, Flint A, Lynch JP 3rd, Martinez FJ (2003) Radiological versus histological diagnosis in UIP and NSIP: survival implications. Thorax 58:143–148
21. Sumikawa H, Johkoh T, Colby TV, Ichikado K, Suga M, Taniguchi H, Kondoh Y, Ogura T, Arakawa H, Fujimoto K, Inoue A, Mihara N, Honda O, Tomiyama N, Nakamura H, Müller NL (2008) Computed tomography findings in pathological usual interstitial pneumonia: relationship to survival. Am J Respir Crit Care Med 177:433–439
22. Daniels CE, Yi ES, Ryu JH (2008) Autopsy findings in 42 consecutive patients with idiopathic pulmonary fibrosis. Eur Respir J 32:170–174
23. Park IN, Kim DS, Shim TS, Lim CM, Lee SD, Koh Y, Kim WS, Kim WD, Jang SJ, Colby TV (2007) Acute exacerbation of interstitial pneumonia other than idiopathic pulmonary fibrosis. Chest 132:214–220
24. Han MK, Murray S, Fell CD, Flaherty KR, Toews GB, Myers J, Colby TV, Travis WD, Kazerooni EA, Gross BH, Martinez FJ (2008) Sex differences in physiological progression of idiopathic pulmonary fibrosis. Eur Respir J 31:1183–1188

25. Alakhras M, Decker PA, Nadrous HF, Collazo-Clavell M, Ryu JH (2007) Body mass index and mortality in patients with idiopathic pulmonary fibrosis. Chest 131:1448–1453
26. Kondoh Y, Taniguchi H, Katsuta T, Kataoka K, Kimura T, Nishiyama O, Sakamoto K, Johkoh T, Nishimura M, Ono K, Kitaichi M (2010) Risk factors of acute exacerbation of idiopathic pulmonary fibrosis. Sarcoidosis Vasc Diffus Lung Dis 27:103–110
27. Seeger W, Adir Y, Barberà JA, Champion H, Coghlan JG, Cottin V, De Marco T, Galiè N, Ghio S, Gibbs S, Martinez FJ, Semigran MJ, Simonneau G, Wells AU, Vachiéry JL (2013) Pulmonary hypertension in chronic lung diseases. J Am Coll Cardiol 62:D109–D116
28. Hachulla E, Gressin V, Guillevin L, Carpentier P, Diot E, Sibilia J, Kahan A, Cabane J, Francès C, Launay D, Mouthon L, Allanore Y, Tiev KP, Clerson P, de Groote P, Humbert M (2005) Early detection of pulmonary arterial hypertension in systemic sclerosis: a French nationwide prospective multicenter study. Arthritis Rheum 52:3792–3800

OPEN ACCESS Freely available online

PLOS | ONE

Estrogen-Dependent Proteolytic Cleavage of Semaphorin 4D and Plexin-B1 Enhances Semaphorin 4D-Induced Apoptosis during Postnatal Vaginal Remodeling in Pubescent Mice

Takuji Ito[1☯], Tao Bai[2☯], Tetsuji Tanaka[2☯], Kenji Yoshida[1], Takashi Ueyama[3], Masayasu Miyajima[4], Takayuki Negishi[1], Takahiko Kawasaki[5], Hyota Takamatsu[6], Hitoshi Kikutani[7], Atsushi Kumanogoh[6], Kazunori Yukawa[1]*

1 Department of Physiology, Faculty of Pharmacy, Meijo University, Nagoya, Japan, **2** Department of Obstetrics and Gynecology, Wakayama Medical University, Wakayama, Japan, **3** Department of Anatomy and Cell Biology, Wakayama Medical University, Wakayama, Japan, **4** Laboratory Animal Center, Wakayama Medical University, Wakayama, Japan, **5** Division of Brain Function, National Institute of Genetics, Graduate University for Advanced Studies (Sokendai), Mishima, Japan, **6** Department of Immunopathology, Research Institute for Microbial Diseases, Osaka University, Suita, Japan, **7** Department of Molecular Immunology, Research Institute for Microbial Diseases, Osaka University, Suita, Japan

Abstract

Around the fifth week after birth, the vaginal cavity in female mouse pups opens to the overlaying skin. This postnatal tissue remodeling of the genital tract occurs during puberty, and it largely depends upon hormonally induced apoptosis that mainly occurs in the epithelium at the lower part of the mouse vaginal cavity. Previously, we showed that most BALB/c mice lacking the class IV Semaphorin (Sema4D) develop imperforate vagina and hydrometrocolpos; therefore, we reasoned that the absence of Sema4D-induced apoptosis in vaginal epithelial cells may cause the imperforate vagina. Sema4D signals via the Plexin-B1 receptor; nevertheless detailed mechanisms mediating this hormonally triggered apoptosis are not fully documented. To investigate the estrogen-dependent control of Sema4D signaling during the apoptosis responsible for mouse vaginal opening, we examined structural and functional modulation of Sema4D, Plexin-B1, and signaling molecules by analyzing both wild-type and Sema4D−/− mice with or without ovariectomy. Both the release of soluble Sema4D and the conversion of Plexin-B1 by proteolytic processing in vaginal tissue peaked 5 weeks after birth of wild-type BALB/c mice at the time of vaginal opening. Estrogen supplementation of ovariectomized wild-type mice revealed that both the release of soluble Sema4D and the conversion of Plexin-B1 into an active form were estrogen-dependent and concordant with apoptosis. Estrogen supplementation of ovariectomized Sema4D−/− mice did not induce massive vaginal apoptosis in 5-week-old mice; therefore, Sema4D may be an essential apoptosis-inducing ligand that acts downstream of estrogen action in vaginal epithelium during this postnatal tissue remodeling. Analysis of ovariectomized mice also indicated that Sema4D contributed to estrogen-dependent dephosphorylation of Akt and ERK at the time of vaginal opening. Based on our results, we propose that apoptosis in vaginal epithelium during postnatal vaginal opening is induced by enhanced Sema4D signaling that is caused by estrogen-dependent structural changes of Sema4D and Plexin-B1.

Citation: Ito T, Bai T, Tanaka T, Yoshida K, Ueyama T, et al. (2014) Estrogen-Dependent Proteolytic Cleavage of Semaphorin 4D and Plexin-B1 Enhances Semaphorin 4D-Induced Apoptosis during Postnatal Vaginal Remodeling in Pubescent Mice. PLoS ONE 9(5): e97909. doi:10.1371/journal.pone.0097909

Editor: Hiroyasu Nakano, Toho University School of Medicine, Japan

Received January 30, 2014; **Accepted** April 25, 2014; **Published** May 19, 2014

Funding: This work was primarily supported by Grants-in-Aid for Scientific Research from the Ministry of Education, Science, Sports and Culture, Japan (#19590178, http://www.jsps.go.jp/j-grantsinaid/index.html), and partly supported by several grants from the Research Institute of Meijo University. The funders had no role in study design, data collection and analysis, decision to publish, or preparation of the manuscript.

Competing Interests: The authors have declared that no competing interests exist.

* E-mail: kyukawa@meijo-u.ac.jp

☯ These authors contributed equally to this work.

Introduction

In mice, the blind ending of the vaginal cavity in each female pup opens to the skin around 5 weeks after birth when sex hormone level rises in the internal environment; vaginal opening is one of very few postnatal tissue remodeling events in mice [1]. The study of transgenic mice that overexpress the human anti-apoptotic protein Bcl-2 in the vaginal mucosa clearly shows that this postnatal tissue remodeling process depends heavily on massive mucosal apoptosis; these cell deaths occur in a very limited time window and only at the lower distal end of mouse vaginal cavity in the vicinity of skin [1]. Subsequently, several studies involving various types of knockout mice revealed the crucial involvement of proapoptotic Bcl2 family proteins [2,3], along with other signaling molecules, in mouse vaginal remodeling [4,5]. However, the exact mechanisms by which rapid increases of estrogen level in the mouse internal environment induce the extensive apoptosis in vaginal epithelium at the time of puberty remain unknown [1,6]. We found that mice lacking Semaphorin 4D (Sema4D) often develop imperforate vagina and hydrometro-

colpos [7]; Sema4D is a semaphorin that controls axon guidance during neuronal development [8,9].

Semaphorins are a family of secreted and transmembrane glycoproteins with phylogenetically conserved domains; they were originally identified as repulsive axon guidance molecules that function during development of the nervous system [10]. Sema4D (also called CD100) is a class 4 transmembrane-type semaphorin that binds to Plexin-B1, which is a transmembrane receptor and a member of the plexin family, to induce repulsive cytoskeletal changes in growth cones of cultured neurons [11]. Sema4D and Plexin-B1 interact via their conserved sema domains of ~400 amino acids each; each sema domain forms a seven-blade β-propeller fold in the extracellular domain of the respective protein [10,12,13]. Binding of Sema4D to Plexin-B1 causes Plexin-B1 molecules to cluster; this clustering facilitates GTPase activating protein (GAP) activities of the two GAP domains in the intracellular region of each Plexin-B1 molecule [14]. The augmented Plexin-B1 GAP activities in neurons 1) downregulate activities of Ras family members and 2) induce dephosphorylation of Akt and ERK and activation of glycogen synthase kinase (GSK)-3β; these events reduce integrin-mediated cell adhesion to the extracellular matrix, and consequently induce morphological remodeling of growth cones and dendrites in cultured neurons [14,15,16]. In contrast, Sema4D binding to Plexin-B1 on endothelial cells stimulates the activation of the phosphatidylinositol 3-kinase (PI3K)-Akt pathway and of ERK to induce endothelial cell migration [17,18]. Thus the Sema4D signal either facilitates or weakens the same intracellular signaling pathway depending upon the cell type and cellular context. Membrane-bound Sema4D on T lymphocytes is cleaved via metalloprotease-dependent proteolysis, and the extracellular domain is then shed as diffusible secreted protein from a membrane surface to the surrounding extracellular environment [19]. Soluble secreted Sema4D is thought to function as a guidance cue that acts across long distances to inhibit immune cell migration [19]. Plexin-B1 is also converted from a precursor into an active heterodimeric form composed of distinct subunits resulting from proprotein convertase-mediated processing of Plexin-B1 [20]. The proteolytically processed, active form of Plexin-B1 transmits a more intense Sema4D-dependent intracellular signal than does the unprocessed precursor [20].

The high frequency of vaginal atresia and the significant attenuation of vaginal epithelial apoptosis in Sema4D-deficient (Sema4D−/−) mice indicates that vaginal mucosal apoptosis and the vaginal opening process do not occur normally in these mice. Furthermore, we demonstrated that Sema4D binds to Plexin-B1 receptor to induce apoptosis of vaginal epithelial cells in culture. β-Estradiol administration in infant Sema4D-deficient mice does not induce precocious vaginal opening; therefore, Sema4D may function downstream of estrogen action during postnatal vaginal tissue remodeling [7]. However, mouse vaginal opening occurs 5 weeks after birth when estrogen levels increase rapidly in female mice, and the pro-apoptotic signals in the maturing vaginal epithelial cells may be enhanced via estrogen-mediated functional modulation of Sema4D and Plexin-B1. Here, we examined whether estrogen induces structural and functional changes in Sema4D and Plexin-B1 that lead to the induction of vaginal epithelial apoptosis and the consequent tissue remodeling. The results of our study indicated 1) that Sema4D cleavage and Plexin-B1 activation were both estrogen dependent and 2) that these events led to vaginal epithelial apoptosis in this postnatal tissue remodeling event.

Materials and Methods

Generation of Sema4D−/− Mice

Sema4D−/− mice generated by gene targeting [21] were backcrossed with BALB/c mice for 10 generations. Pairs of resultant heterozygous mice were bred to obtain homozygous, knockout mice and their wild-type (WT) littermates. The mice were bred for the preparatory and pairwise in the animal facilities of Wakayama Medical University and the animal center in the Faculty of Pharmacy, Meijo University. Each researcher and each laboratory technician followed the guidelines promulgated by the Physiological Society of Japan and the respective guidelines on animal experiments from Wakayama Medical University and from Meijo University when caring for or sacrificing mice and when conducting protocols involving mice. Each institutional Animal Ethics Review committee, the Wakayama Medical University committee and the Meijo University committee, approved the experimental protocols (approval number: 267; Wakayama Medical University, 2012-yaku-jitsu-8; Meijo University).

Genotype Analysis

Mouse tail DNA, Sema4D gene-specific primers, and PCR were used as described previously to determine each mouse genotype [21].

Immunohistochemistry and TUNEL Assay

Mice were sacrificed by intraperitoneal injection of pentobarbital sodium (Kyoritsuseiyaku Co., Tokyo, Japan) and then subjected to transcardiac perfusion of 4% paraformaldehyde. Each vagina excised from a mouse was fixed overnight in 4% paraformaldehyde solution. Each vagina was then embedded longitudinally in paraffin and cut into 4-μm serial sections. Sections were immunolabeled with anti-cleaved caspase-3 (Cell Signaling Technology, Beverly, MA), anti-Akt (Cell Signaling Technology), or anti-Erk1/2 antibody (Cell Signaling Technology). TUNEL assays were performed basically as described previously [22], using a fluorometric TUNEL assay system (Promega, Madison, WI) following the manufacturer's protocols.

Western Blot

To reduce the variance among samples, dissection of each mouse vagina was conducted as follows. A mouse was sacrificed via intraperitoneal injection of pentobarbital sodium; a laparotomy was then performed to expose the reproductive organs, and the fatty tissues around the vagina were then removed. The pubic bone was resected to view the lower region of the vagina; the urinary bladder, urethra, and rectum were then separated from the vagina. In each case of an unopened vagina, the border area between the lowest end of the vagina and the skin surface of the expected vaginal orifice was transversely cut so that the septum covering the lower extremity of the vagina [1] was included in the vaginal tissue sample; simultaneously, the uterine cervix was pulled ventrally with forceps. In each case of an opened vagina, the region between the vaginal orifice and the surrounding skin was cut while the uterine cervix was pulled ventrally with forceps. Each vagina was obtained via a transverse cut beneath the lowest extremity of the uterine cervix to exclude the cervix; each such vagina was rapidly minced into small pieces on ice. Tissue extracts were prepared by homogenizing the mouse vaginal tissue in T-PER Tissue Protein Extraction Reagent (Thermo Scientific Inc., Waltham, MA) with a protease inhibitor, α-complete (Roche Applied Science, Penzberg, Germany), and a phosphatase inhibitor, PhosStop (Roche Applied Science). The Bio-Rad Protein assay (Bio-Rad, Hercules, CA) was used to measure the

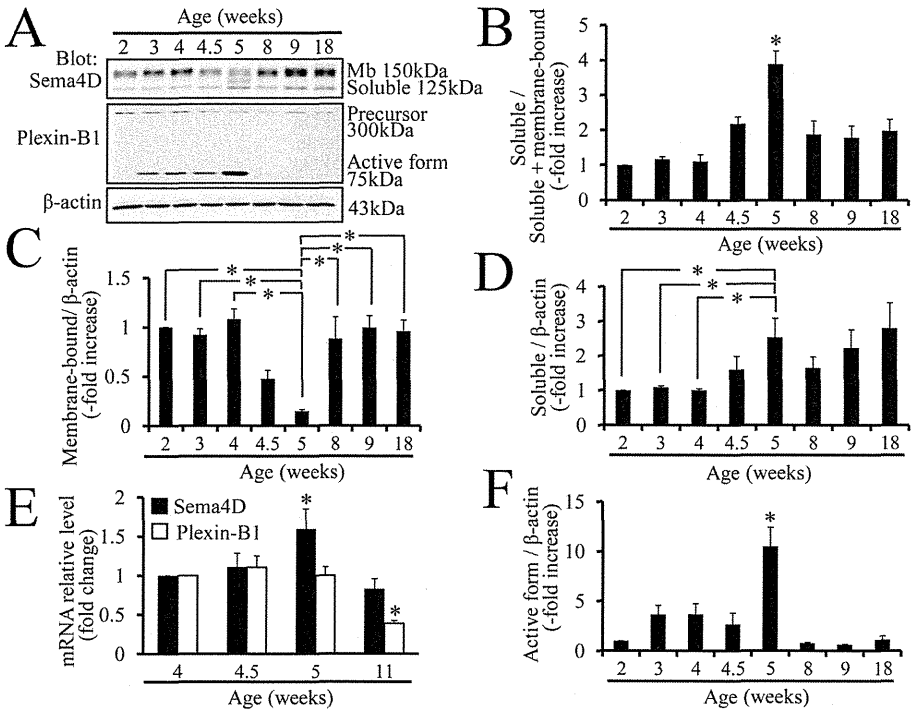

Figure 1. Increase of soluble Sema4D and reorganization of Plexin-B1 receptor during vaginal development. (A) The membrane-bound (larger) and soluble (smaller) forms of Sema4D are evident on western blots containing proteins from vaginal tissue extracts. The precursor (larger) and active form (smaller) of Plexin-B1 are also evident on western blots containing proteins from vaginal tissue extracts; the active 75 kDa form represents a fragment of the 300 kDa Plexin-B1 precursor produced by proprotein convertase. The fragments resulting from the proprotein convertase-dependent cleavage are integrated into signaling-active receptors, which have a distinct conformation from the precursors [20]. Age (weeks): vaginal protein extracts from 2-, 3-, 4-, 4.5-, 5-, 8-, 9-, or 18-week-old mice. Mb: membrane-bound. (B) The ratio of soluble Sema4D to total Sema4D increases significantly in 5-week-old mouse vaginal tissue. Each data point represents the mean ± SEM of 3 to 6 mice. *$P<0.05$, ANOVA. (C) The ratio of membrane-bound Sema4D to β-actin significantly decreases in 5-week-old vaginal tissue. Each column represents the mean ± SEM of 4 mice. *$P<0.05$, ANOVA. (D) The ratio of soluble Sema4D to β-actin in 5-week-old mouse vaginal tissue is significantly higher than that in 2-, 3-, or 4-week-old mouse vaginal tissue. Each value represents the mean ± SEM of 3 to 6 mice. *$P<0.05$, ANOVA. (E) Based on real-time PCR data, the expression of Sema4D mRNA increases significantly in vaginal tissue from 5-week-old mice as compared with that from any other developmental stage. Plexin-B1 mRNA levels show no changes during vaginal opening except for a significant decline in 11-week-old mice. Each column represents the mean ± SEM of 4 mice. *$P<0.05$, ANOVA. (F) The ratio of active Plexin-B1 to β-actin is significantly higher in 5-week-old mouse vaginal tissue than in that from any other developmental stage. Each point represents the mean ± SEM of 3 to 6 mice. *$P<0.05$, ANOVA.
doi:10.1371/journal.pone.0097909.g001

protein content in each tissue extract, and samples containing 15 μg of protein were prepared with a solution of 60 mM Tris-HCl (pH 6.8), 2% SDS, 10% glycerol, 0.1% bromophenol blue, and 5% β-mercaptoethanol; each of these samples was incubated at 100°C for 5 min and subjected to electrophoresis through a 10% SDS-polyacrylamide gel; separated proteins were then transferred to polyvinylidine difluoride membranes (Amersham Pharmacia Biotech, Buckinghamshire, UK). Sema4D, plexin-B1, cleaved caspase-3, Akt, phospho-Akt, ERK1/2, and phospho-ERK1/2 were detected with the respective antibodies and an ECL-plus or ECL Western blot detection system in accordance with the manufacturers' instructions (Amersham). The antibodies utilized were anti-CD100/Sema4D (BD Transduction Laboratories, NJ, USA), anti-plexin-B1 (Santa Cruz Biotechnology, Inc.), anti-cleaved caspase-3 (Cell Signaling Technology), anti-Akt (Cell Signaling Technology), anti-phospho-Akt (Cell Signaling Technology), anti-Erk1/2 (Cell Signaling Technology), anti-phospho-Erk1/2 antibody (Cell Signaling Technology), and β-actin antibody (Cell Signaling Technology).

Ovariectomy and Estrogen Supplementation

For each ovariectomy (OVX), both ovaries were excised from a 22-day-old mouse while the mouse was under anesthesia from intraperitoneal injection of pentobarbital sodium. As controls, sham operations, in which both ovaries were manipulated but not resected, were performed on WT or Sema4D−/− mice. Ovariectomized mice were then separated into three groups: in two groups, from postnatal day 24 to postnatal day 34, β-estradiol (E2, 0.1 μg/kg body weight, Sigma Chemical Co., St. Louis, MO) (OVX-E2 group) or vehicle oil (OVX-oil group) was injected daily and subcutaneously into each mouse, and in the remaining group, no injection was administered (OVX group). The OVX-E2 and OVX-oil groups were sacrificed for Western and immunohistochemical analysis 24 hours after the last injection. Both sham-operated and OVX mice were also sacrificed for Western and immunohistochemical analysis on postnatal day 35. Uterine weight of each mouse was measured to assess the effects of OVX, oil supplementation (OVX-oil) and estrogen supplementation (OVX-E2), as shown in Fig. S1.

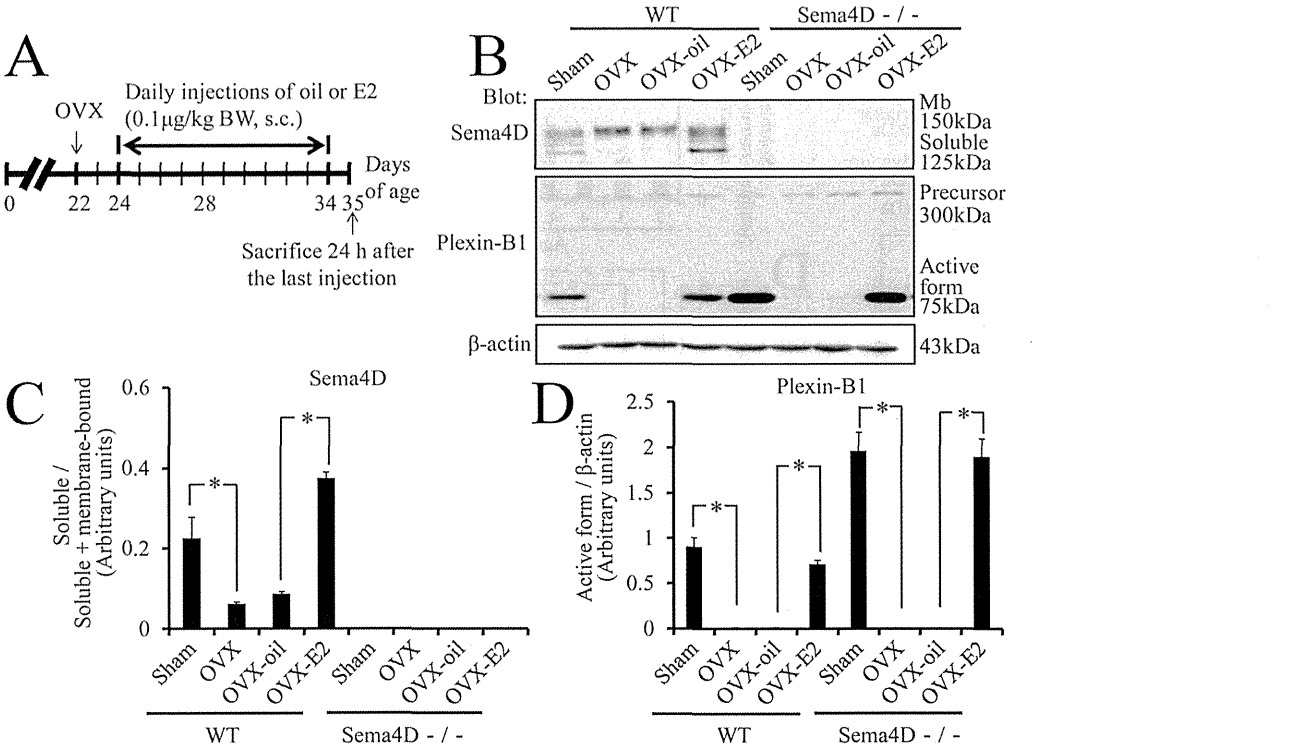

Figure 2. Hormonal regulation of structural changes in Sema4D and Plexin-B1. (A–D) To investigate whether estrogen induces structural changes in Sema4D, Plexin-B1, or both, ovariectomized mice receive daily subcutaneous injections (s.c.) of 17β-estradiol (E2, 0.1 μg/kg) until 5 weeks after birth. As expected, both soluble Sema4D and active Plexin-B1 are detected in vaginal tissue from sham-operated 5-week-old female WT mice (Sema4D+/+). Interestingly, after ovariectomy (OVX) and ovariectomy plus oil supplementation (OVX-oil), the amounts of both soluble Sema4D and active Plexin-B1 significantly decrease. The decrease in active protein levels is rescued by daily subcutaneous injection of E2 (OVX-E2); these findings indicate that the enzymes cleaving membrane-type Sema4D and Plexin-B1 precursor are induced by estrogen. In Sema4D−/− mice, OVX and OVX-oil result in significant decreases in the active form of Plexin-B1; these decreases are abrogated by OVX-E2 treatment. Both membrane-bound and soluble Sema4D are not evident in samples from Sema4D−/− mice. Each value in the graphs (C, D) represents the mean ± SEM of 5 mice. *$P<0.05$, ANOVA.
doi:10.1371/journal.pone.0097909.g002

Real-time RT-PCR

The SV Total RNA Isolation System (Promega, Madison, WI) was used according to the manufacturer's instructions to extract RNA from vaginal tissues of sham-operated WT and Sema4D−/− mice, as well as from OVX, OVX-oil, and OVX-E2 mice. Total RNA was extracted from developing vaginal tissues via the same procedure. The QuantiTect Primer Assays and the following probes Mm_Sema4d_1_SGQT00115206, Mm_Plxnb1_1_SG QT00126483, Mm_B2m_2_SG QT01149547 (Qiagen, Tokyo, Japan) were used according to the manufacturer's instructions to perform real-time RT-PCR.

Statistics

Each data value was expressed as a mean ± standard error of the mean (SEM). Comparisons between WT and Sema4D−/− mice were conducted with the Student's t-test or a one-way or two-way analysis of variance (ANOVA) followed by a *post hoc* test. A level of $p<0.05$ was considered statistically significant.

Results

Conversion of Membrane-bound Sema4D to Soluble Secreted Sema4D during Vaginal Development

Western blots were probed with anti-Sema4D antibodies to examine the expression patterns of membrane-bound and soluble secreted Sema4D during vaginal development; samples of tissue extracts were taken from each stage of postnatal mouse vaginal development. The ratio of soluble to total Sema4D was significantly higher 5 weeks after birth, which is when vaginal opening occurs, than at any other developmental stage (Fig. 1A, B). Membrane-bound Sema4D level was significantly lower at 5 weeks after birth than at any other developmental stage (Fig. 1C). The results illustrated that the rate of conversion from membrane-bound Sema4D to secreted Sem4D was significantly higher at the time of vaginal opening than at any other developmental stage.

Concordant with the significantly higher level of soluble secreted Sema4D in 5-week-old vaginal tissues, the *Sema4D* mRNA level was also significantly higher in 5-week-old vagina tissue based on real-time RT-PCR analysis (Fig. 1E).

Reorganization of Plexin-B1 during Vaginal Development

Western blots were probed with anti-Plexin-B1 antibodies to examine whether the expression of the Sema4D receptor, Plexin-B1, changed during vaginal development. Vaginal tissue protein extracts from each developmental stage and anti-Plexin-B1 antibodies that detected both a 300 kDa form and a smaller 75 kDa form were used for this analysis (Fig. 1A). The 300 kDa protein represents the precursor form of Plexin-B1 that exists prior to digestion by a protease, proprotein convertase [20]. The smaller 75 kDa protein represents the Plexin-B1 fragment that is

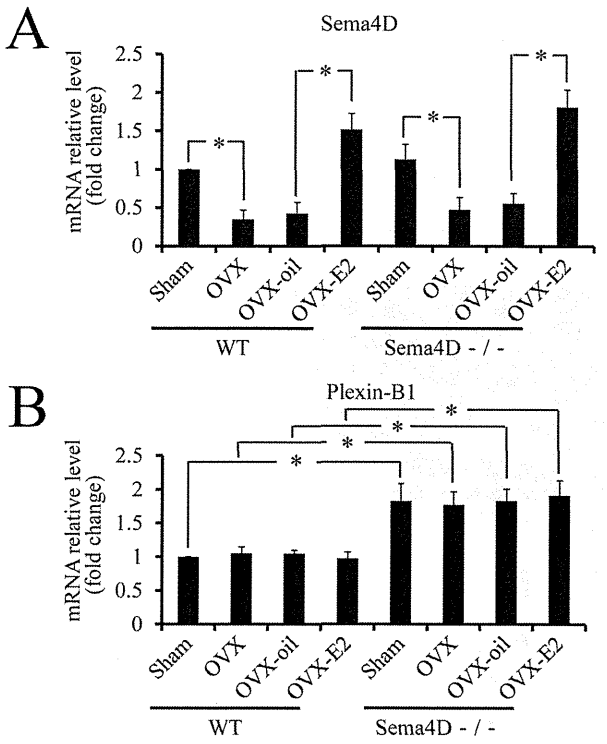

Figure 3. Estrogen increases levels of *Sema4D* mRNA, but not *Plexin-B1* mRNA in mouse vagina. (A) *Sema4D* mRNA levels were significantly lower in vaginal tissues from OVX WT mice than in vaginal tissues from sham-operated mice. Based on comparisons between OVX-E2 and OVX-oil mice, OVX-E2 treatment induced a significant increase of *Sema4D* mRNA levels in WT vaginal tissues. The *Sema4D* mRNA variant transcribed in Sema4D−/− mice, but not translated into Sema4D protein exhibits an expression pattern similar to that of wild-type *Sema4D* mRNA. Each value represents the mean ± SEM of 5 mice. *$P<$ 0.05, ANOVA. (B) *Plexin-B1* mRNA levels in vaginal tissues from any Sema4D−/− mice group were significantly higher than those in vaginal tissues from any WT mice group. In WT or Sema4D−/− mice, any treatment does not induce any significant alteration of *Plexin-B1* mRNA levels in vaginal tissues. Each value represents the mean ± SEM of 5 mice. *$P<0.05$, ANOVA.
doi:10.1371/journal.pone.0097909.g003

generated by proprotein convertase-mediated digestion [20]. After convertase-mediated digestion of the Plexin-B1 precursor, the conformation of Plexin-B1 protein structure is transformed into an active form that transmits Sema4D signal more intensely (20, Fig. S2). Interestingly, the ratio of the smaller 75 kDa band to the β-actin band was significantly higher for the 5-week sample than for any other sample (Fig. 1F). Thus the western blot findings indicated that the active form of Plexin-B1 was highest at 5 weeks, which is the time of mouse vaginal opening. Real-time PCR analysis demonstrated that *Plexin-B1* mRNA levels were constant during postnatal vaginal development except that the mRNA declined significantly by the 11th week (Fig. 1E).

Conversion of Sema4D and of Plexin-B1 is Estrogen-dependent

Postnatal vaginal remodeling in mice is a hormonally triggered process [1]; therefore, we investigated whether proteolytic release of Sema4D and reorganization of Plexin-B1 during remodeling were each estrogen dependent. Mice were initially subjected to ovariectomy on postnatal day 22; one third of these mice were each injected with exogenous estrogen (OVX-E2 mice), another third with vehicle only (OVX-oil mice, Fig. 2A) and the remaining third received no injection (OVX mice). Western blot analysis was used to examine both Sema4D proteolysis and Plexin-B1 conversion in these ovariectomized mice when the mice became 5 weeks old (Fig. 2B). Conversion of membrane-bound Sema4D into the soluble form was significantly lower in OVX mice than in sham-operated WT mice (Fig. 2B, C). In contrast, this Sema4D conversion was significantly higher in WT OVX-E2 than in WT OVX-oil mice (Fig. 2B, C); these findings indicated that proteolytic conversion of Sema4D was estrogen dependent. Reorganization of Plexin-B1 into an active form was significantly lower in WT OVX mice than in sham-operated WT mice (Fig. 2B, D). The reorganization of Plexin-B1 was significantly higher in WT OVX-E2 mice than in WT OVX-oil mice; these findings indicated Plexin-B1 reorganization during mouse vaginal tissue remodeling was estrogen dependent (Fig. 2B, D). The phenomenon was also confirmed in Sema4D−/− mice (Fig. 2B, D).

To examine whether OVX and OVX-E2 treatment affected *Sema4D* or *Plexin-B1* mRNA expression, or both, *Sema4D* and *Plexin-B1* mRNA levels in vaginal tissues were quantified via real-time RT-PCR for sham-operated WT and Sema4D−/− mice, as well as OVX mice, OVX-oil mice and OVX-E2 mice. *Sema4D* mRNA levels in vaginal tissues from WT OVX mice were significantly lower than in vaginal tissues from WT sham-operated mice. Conversely, *Sema4D* mRNA levels were significantly higher in vaginal tissues from OVX-E2 WT mice than vaginal tissues from OVX or OVX-oil mice (Fig. 3A); these findings indicated that estrogen mediated transcriptional modulation of *Sema4D* gene. Real-time PCR with forward and reverse primers corresponding to nucleotide sequences in the second and third exons of the *Sema4D* gene, respectively, detected a *Sema4D* mRNA variant in Sema4D−/− vagina tissues (Fig. 3A). The *Sema4D* mRNA variant did not contain the region transcribed from the coding sequences in the first exon of the *Sema4D* gene because the coding sequences covering the translation-initiation codon are not found in the Sema4D−/− mice genome [21]. Thus, the *Sema4D* mRNA variant was not translated to Sema4D protein. Indeed, the Sema4D protein could not be detected in the Sema4D−/− vagina (Fig. 2B, C) or in Sema4D−/− immune cells [21]. Levels of this mRNA variant were significantly higher in Sema4D−/− vaginal tissues from OVX-E2 mice than in vaginal tissues from OVX or OVX-oil mice (Fig. 3A); these findings indicated that estrogen mediated transcriptional modulation of this *Sema4D* mRNA variant. *Plexin-B1* mRNA levels in vaginal tissues from sham-operated Sema4D−/− mice, as well as OVX, OVX-oil, and OVX-E2 mice, were significantly higher than *Plexin-B1* mRNA levels in any WT group (Fig. 3B). However, neither OVX nor OVX-E2 treatment significantly altered *Plexin-B1* mRNA levels in the vaginal tissues of WT or Sema4D−/− mice (Fig. 3B). Thus, the increase of Plexin-B1 reorganization into an active form in vaginal tissues of OVX-E2 mice resulted from an increase in the estrogen-dependent cleavage of Plexin-B1 precursor.

Sema4D is Integral for Estrogen-dependent Vaginal Epithelial Apoptosis *In vivo*

To determine whether Sema4D is essential to vaginal epithelial apoptosis *in vivo*, we measured and compared apoptosis in WT and Sema4D−/− mice; these mice were ovariectomized or sham-operated 3 weeks after birth and then treated with estrogen or vehicle until 5 weeks after birth. Caspase-3 activation was used to measure vaginal apoptosis, and caspase-3 activation was significantly higher in WT OVX-E2 mice than in WT OVX-oil mice (Fig. 4A, C). In contrast, based on both western blot analysis and

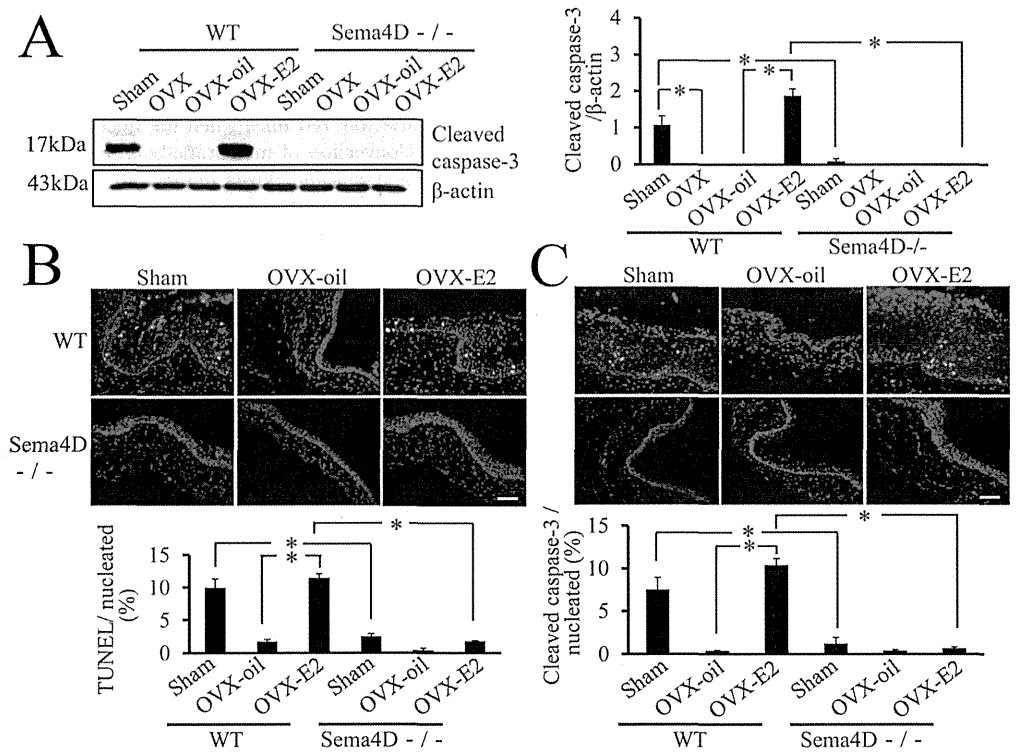

Figure 4. Essential role of Sema4D in estrogen-mediated vaginal apoptosis. (A) Both OVX and OVX-oil treatment of WT (Sema4D+/+) mice result in a significant decrease in cleaved caspase-3 level in vaginal tissue relative to cleaved caspase-3 levels in sham-operated mice (Sham). All vaginal tissue samples were taken from 5-week-old mice. Levels of cleaved caspase-3 were significantly higher in vaginal tissues from WT OVX-E2 mice than in vaginal tissues from WT OVX or WT OVX-oil mice. Levels of cleaved caspase-3 in vaginal tissue did not differ among OVX, OVX-E2, and OVX-oil Sema4D−/− mice; these findings indicate that Sema4D is essential to estrogen-mediated vaginal apoptosis. Each value represents the mean ± SEM of 5 mice. *$P<0.05$, ANOVA. (B, C) Both TUNEL assays and cleaved caspase-3 immunohistochemistry with vaginal tissue sampled from sham-operated (Sham) 5-week-old WT female (Sema4D+/+) mice show that the number of apoptotic epithelial cells is significantly larger than that in samples from Sham-treated Sema4D−/− mice. OVX-oil treatment of WT mice significantly decreases apoptotic cell number in 5-week-old vaginal epithelia relative to that in Sham; compared with OVX-oil treatment, OVX-E2 treatment of WT mice induces a significant increase in apoptotic cell number in 5-week-old vaginal epithelia, comparable to the level of Sham. OVX-E2 treatment does not induce significant apoptosis in 5-week-old vaginal epithelia of Sema4D−/− mice. Data are shown as means ± SEM; n = 5 per group.
doi:10.1371/journal.pone.0097909.g004

immunohistochemistry, vaginal apoptosis in ovariectomized Sema4D−/− mice remained low even in Sema4D−/− OVX-E2 mice (Fig. 4A, B, C). The results indicated that Sema4D was essential for estrogen-dependent vaginal epithelial cell apoptosis *in vivo* during the postnatal vaginal tissue remodeling that occurs 5 weeks after birth.

Dephosphorylation of Akt and ERK at the Time of Vaginal Opening is an Estrogen-dependent, Sema4D-mediated Event in Vaginal Epithelium

The mechanism suppressing activation of Akt and ERK may operate downstream of semaphorin signaling [16,23]; therefore, we examined the localization of Akt and ERK in the mouse vagina. Immunohistochemical findings indicated that these molecules were present in vaginal epithelium of WT and of Sema4D−/− mice (Fig. 5A). To examine whether dephosphorylation of Akt and of ERK operates in vaginas of 5-week-old WT mice, we used western blots to measure phosphorylated and unphosphorylated forms of these proteins during mouse vaginal development. The levels of both p-Akt and p-ERK decreased significantly in vaginas of 5-week-old WT mice at the time of vaginal opening; these findings indicated that Sema4D signal suppressed phosphorylation-dependent activation of Akt and of ERK (Fig. 5B).

To examine whether the decreases in p-Akt and in p-ERK depended on Sema4D, we compared WT and Sema4D−/− mice with regard to the levels of p-Akt and p-ERK in vaginal epithelium 5 weeks after birth. Western blot analysis showed that p-Akt and p-ERK expression was significantly higher in the Sema4D−/− vaginal tissue than in WT vaginal tissue (Fig. 5C). Thus, Sema4D signal may induce dephosphorylation of Akt and ERK at the time of vaginal opening.

To determine whether the decreases in p-Akt and p-ERK expression in mouse vaginal tissue 5 weeks after birth are estrogen dependent and Sema4D mediated, we measured p-Akt and p-ERK levels in vaginal tissues from WT and from Sema4D−/− mice that had been ovariectomized or sham-operated 3 weeks after birth and treated with vehicle only or estrogen thereafter. In vaginal tissue of WT mice, p-Akt and p-ERK expression 5 weeks after birth was significantly higher in OVX mice than in sham-operated mice (Fig. 6). On western blots, p-Akt and p-ERK levels were significantly lower in vaginal tissues from 5-week-old WT OVX-E2 mice than in those from OVX mice or from OVX-oil mice (Fig. 6); these findings indicated that regulation of dephosphorylation of Akt and ERK was estrogen dependent. To

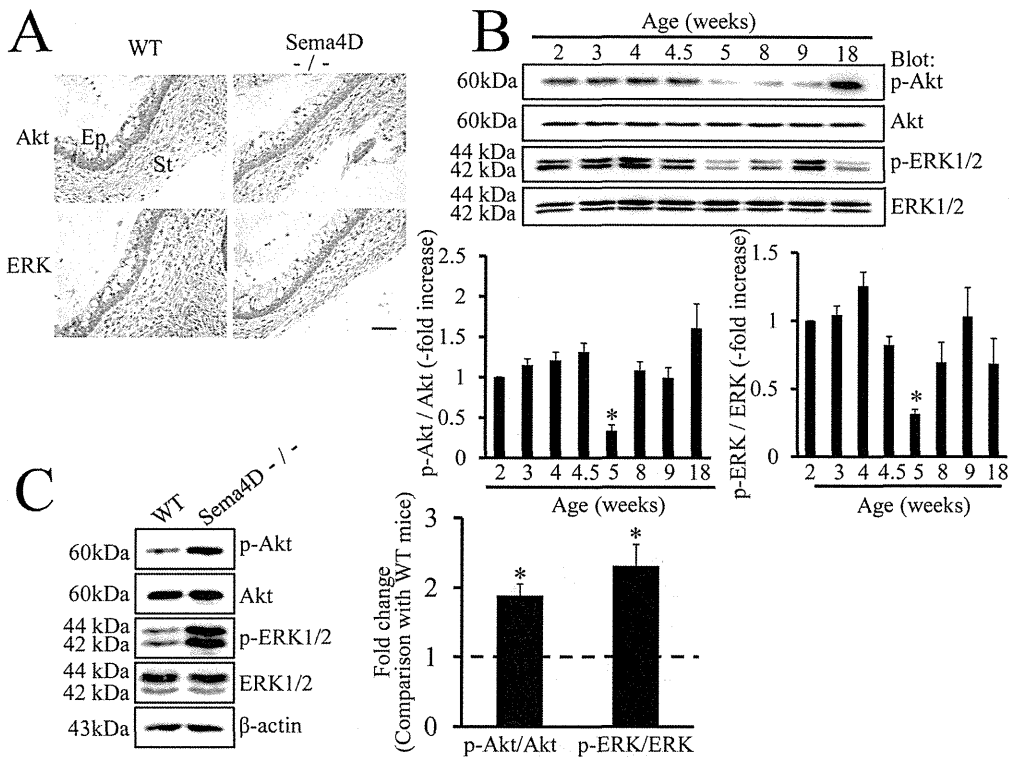

Figure 5. Dephosphorylation of Akt and ERK during vaginal opening. (A) Immunohistochemistry demonstrates that Akt and ERK are expressed in vaginal epithelium of both WT (Sema4D+/+) and Sema4D−/− mice at 5 weeks old at the time of vaginal opening. (B) Western blots show the expression patterns of Akt, ERK, and the respective phosphorylated forms during postnatal vaginal development in WT mice. Both pAkt and pERK levels are lower in samples from 5-week-old mice than in samples from any other stages of development. Age (weeks): vaginal protein extracts from 2-, 3-, 4-, 4.5-, 5-, 8-, 9-, or 18-week-old mice. Each value represents the mean ± SEM of 6 mice. *$P<0.05$, ANOVA. (C) Western blot analysis reveals significantly higher expression of pAkt and pERK in vaginal tissue samples from 5-week-old Sema4D−/− mice than in vaginal tissue samples from 5-week-old WT (Sema4D+/+) mice. The ratios of pAkt to Akt and separately of pERK to ERK were higher in vaginal tissue samples from 5-week-old Sema4D−/− than in vaginal tissue samples from WT mice. Data are shown as the mean ± SEM; n = 6 per mouse group. *$P<0.05$, Student's t-test.
doi:10.1371/journal.pone.0097909.g005

determine the extent to which this change in Akt and ERK phosphorylation depended on Sema4D, we examined tissues from Sema4D−/− mice. Notably, for Sema4D−/− mice, phosphorylation levels of Akt and ERK did not differ significantly among vaginal tissues from sham-operated, OVX, and OVX-oil mice (Fig. 6). However, Akt and ERK phosphorylation in vaginal tissue was significantly lower in Sema4D−/− OVX-E2 mice than in Sema4D−/− OVX-oil mice, but the Akt and ERK phosphorylation in Sema4D−/− OVX-E2 mice was significantly higher than that in WT OVX-E2 mice (Fig. 6). These results indicated that normal estrogen-dependent dephosphorylation of Akt and ERK at the time of vaginal opening was partially, but not completely, dependent on Sema4D.

Discussion

Using Sema4D−/− BALB/c mice, we documented three novel, crucial observations regarding the estrogen-dependent apoptosis that occurs during postnatal vaginal opening in mice. We found that 1) Sema4D, which is classified as a class 4 semaphorin, played an indispensable role as a downstream effector of estrogen action during apoptosis of vaginal epithelial cells as the vagina opens; 2) estrogen-dependent Sema4D processing and estrogen-dependent Plexin-B1 reorganization increased Sema4D signal transduction efficiency during vaginal opening; and 3) Sema4D contributed to estrogen-dependent attenuation of both Akt and ERK signaling during vaginal opening.

The high incidence of imperforate vagina and the prominent decrease in vaginal epithelial apoptosis during puberty in Sema4D−/− mice led to the hypothesis that Sema4D could induce apoptosis of vaginal epithelial cells. Our previous findings regarding Sema4D−/− vaginal epithelial cells in culture demonstrate the apoptosis-inducing activity of Sema4D [7]. Similarly, Sema3A, a member of class 3 semaphorins, induces apoptosis of kidney podocytes [24]. Notably, Sema4D could promote apoptosis of oligodendrocytes to control the differentiation of oligodendrocytes [25]. Furthermore, Sema3A has been implicated in Fas-mediated apoptosis; specifically, it may help the Fas molecule migrate into lipid rafts [26]. Thus, semaphorins exhibit crucial roles not only in axon guidance, but also in induction of apoptosis during development. However, the receptor and signal transduction machinery involved in semaphorin-mediated apoptosis have not been explored in detail. Our previous findings indicate that Plexin-B1 is involved in Sema4D-induced apoptosis of vaginal epithelial cells in culture [7]. In WT ovariectomized mice, apoptosis in vaginal epithelia was significantly higher in the OVX-E2 mice than in vehicle-treated ovariectomized mice (Fig. 4). In contrast, OVX-E2 treatment did not induce significant apoptosis in 5-week-old vaginal epithelia of Sema4D−/− mice (Fig. 4). Thus, these data indicated that Sema4D functioned as an essential downstream effector of estrogen action mediating vaginal

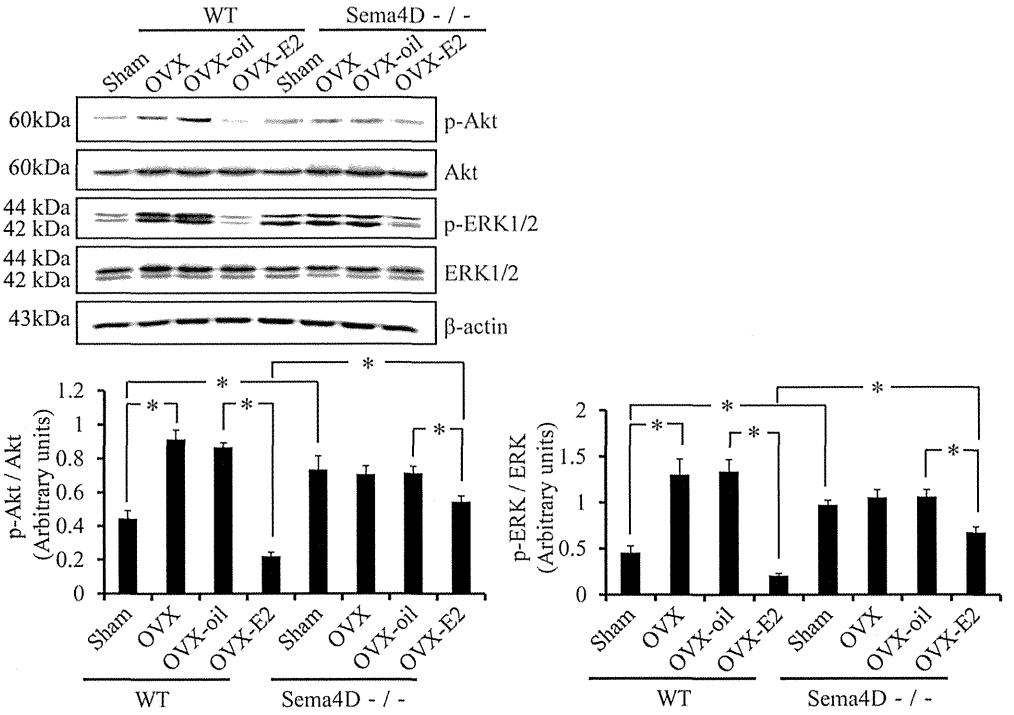

Figure 6. Sema4D contributes to the estrogen-dependent dephosphorylation of Akt and ERK during mouse vaginal opening. Western blot shows that ovariectomy (OVX) and ovariectomy plus oil (OVX-oil) both increase the phosphorylation level of Akt and ERK1/2 in vaginal tissue from 5-week-old WT (Sema4D+/+) mice. β-estradiol (E2) supplementation after ovariectomy (OVX-E2) induces significant dephosphorylation of Akt and ERK1/2 in vaginal tissue from 5-week-old WT mice. OVX and OVX-oil do not significantly increase phosphorylation of Akt and ERK1/2 in vaginal tissue from 5-week-old Sema4D−/− mice relative to that in sham-operated mice (Sham). OVX-E2 induces weak but significant dephosphorylation of Akt and ERK in vaginal tissue from 5-week-old Sema4D−/− mice. Dephosphorylation levels in the Sema4D−/− vagina is significantly lower than that in the WT vagina. Each data point represents the mean ± SEM of 3 to 6 mice. *$P<0.05$, ANOVA.
doi:10.1371/journal.pone.0097909.g006

epithelial apoptosis *in vivo* during postnatal tissue remodeling. Thus, this is the first manuscript reporting that a semaphorin known as an axon guidance molecule exhibited a decisive role in the downstream effects of estrogen action in the process of mouse vaginal opening [1]. Our study of ovariectomized mice further revealed that Sema4D was involved in the estrogen-dependent dephosphorylation of pAkt and pERK in postnatal vaginal tissue remodeling (Fig. 6). Similar to the signal transduction pathway of Sema4D that functions in neuronal growth cone guidance [14,15,16], the Sema4D pathway in vaginal epithelium may involve dephosphorylation of pAkt and pERK; this dephosphorylation may depend on downregulation of Ras family members; this Ras family downregulation may in turn be caused by Plexin-B1 GAP activities that are activated by Sema4D signal in vaginal epithelial apoptosis during vaginal opening in mice.

Conversion of membrane-bound Sema4D to secreted Sema4D was significantly higher during vaginal opening than during any other period of development (Fig. 1A, B, C, D). The increase in the conversion of membrane-bound Sema4D to secreted Sema4D may facilitate induction of apoptosis by increasing the activity of Sema4D as a ligand that acts on both neighboring and distant cells [19]. Sema4D mRNA levels peaked in vaginal epithelium 5 weeks after birth (Fig. 1E); this increase may have boosted apoptosis by increasing ligand quantity. Based on comparisons between OVX-E2 and OVX-oil mice, OVX-E2 treatment induced a significant increase in *Sema4D* mRNA levels in mouse vagina (Fig. 3A), indicating that estrogen may have modulated transcription of the *Sema4D* gene. Since the ratio of soluble Sema4D to total Sema4D increased in concert with the increase of *Sema4D* mRNA in vaginal tissues of WT OVX-E2 mice (Fig. 2B, C), the significant increase in soluble Sema4D in OVX-E2 mice relative to that in OVX-oil mice resulted from enhanced estrogen-dependent cleavage of membrane-bound Sema4D to soluble Sema4D in vaginal tissues in OVX-E2 mice relative to that in OVX-oil mice. Accordingly, experiments involving ovariectomy demonstrated that the conversion from membrane-bound to secreted Sema4D was estrogen dependent (Fig. 2B, C); therefore, the activities and/or amounts of cleavage enzyme releasing soluble Sema4D by cutting membrane-bound Sema4D may increase in response to the estrogen increase at the time of vaginal opening. Although a previous study reported that the function of the cleavage enzyme is to produce the secreted form of Sema4D by cutting membrane-bound Sema4D during T cell activation in the immune system [19], the present study is the first to demonstrate the estrogen-dependent conversion of Sema4D from a membrane-bound precursor to a secreted protein.

Expression of a short fragment of Plexin-B1 that results from enzyme-dependent proteolysis of a Plexin-B1 precursor peaked at the time of vaginal opening; this pattern was similar to the pattern of soluble Sema4D production (Fig. 1A, F). Research with human cell lines showed that a proprotein convertase cleaves the precursor of Plexin-B1 and results in a conformational change of the Plexin-B1 molecule and enhancement of Plexin-B1-mediated signal transduction [20]. Sites that contain the amino acid sequence RXXR and that may be recognized by proprotein convertases actually reside in the mouse Plexin-B1 molecule (R_{546}EERR and R_{1169}GPR, Figure S2). The predicted molecular

size of the cleavage Plexin-B1 molecule produced by proprotein convertases coincides with the size actually detected on western blots probe with anti-Plexin-B1 antibodies (Fig. 1A, Figure S2). The activated form of Plexin-B1, structurally modified and activated for signaling by the proteolytic cleavage, increased most in amount at the time of vaginal opening; this proteolytic conversion may have accelerated vaginal epithelial apoptosis by enhancing signal transduction of Sema4D. Conversion of Plexin-B1 precursor into active Plexin-B1 in mouse vaginal tissue was estrogen dependent (Fig. 1A, Fig. 2B, D); therefore, the amounts and/or activities of the proprotein convertases that cleave Plexin-B1 may also increase in an estrogen-dependent manner. Even though the receptor activation that is mediated by the proteolytic cleavage of Plexin-B1 was previously observed in several cultured cell lines [20], our study is the first to demonstrate the estrogen dependency of the proteolytic conversion of Plexin-B1 during mouse vaginal opening.

C57BL/6 Sema4D−/− mice do not exhibit a high incidence of imperforate vagina, but BALB/c Sema4D−/− mice do. LH-RH neuron precursor cells in C57BL/6 Sema4D−/− mice exhibit defective migration from the olfactory placode to the hypothalamus during embryonic brain development [27]. A significant decrease in secondary ovarian follicles is also evident in Sema4D−/− C57BL/6 mice [28]. Our previous study revealed no significant difference in serum estrogen levels between Sema4D−/− BALB/c mice and WT mice 5 weeks after birth. [7]. Since injection of β-estradiol into infant Sema4D−/− mice does not lead to vaginal opening, the possibility that vaginal atresia in pubescent Sema4D−/− mice was caused by insufficient secretion of estrogen was excluded [7]. Further experiments involving ovariectomy, estrogen supplementation, and WT and Sema4D−/− BALB/c mice clearly revealed that the Sema4D was essential to vaginal epithelial apoptosis, which was regulated by the estrogen present during vaginal opening (Fig. 4A, B, C). Previous findings indicate that Plexin-B1 is the receptor that induces apoptosis of vaginal epithelial cells in culture [7]; however, a closed vaginal phenotype has not been reported in Plexin-B1−/− C57BL/6 mice [29,30]. Future experiments may be necessary to examine whether the closed vaginal phenotype also occurs in BALB/c mice lacking Plexin-B1. The structural conversion of Sema4D and of Plexin-B1 that was evident in BALB/c mice was also evident in C57BL/6 mice during postnatal vaginal development (Fig. S3). However, the day of vaginal opening (5 weeks old) coincided with the peak in the conversion of both Sema4D and Plexin-B1 in BALB/c mice, (Figure 1), but there was no concordance between the day of vaginal opening (37.18 ± 0.787 day old, $n = 17$) and the peak of the proteolytic conversions (24 to 28 days old) in C57BL/6 mice (Fig. S3). These observations may illustrate that postnatal vaginal tissue remodeling processes are more dependent on Sema4D/Plexin-B1 signal transduction system in BALB/c mice than in C57BL/6 mice.

Thus, we propose that extensive apoptosis that occurs in epithelial cells in the vaginal cavity during postnatal vaginal opening in BALB/c mice is induced by Sema4D–Plexin-B1 signaling and that this signaling is enhanced by the estrogen-dependent increase in both soluble Sema4D and active Plexin-B1 5 weeks after birth.

Supporting Information

Figure S1 Confirmation of the effect of ovariectomy and estrogen supplementation. Both ovariectomized (OVX) WT (Sema4D+/+) and Sema4D−/− mice exhibit a significant decrease in uterine weight when compared with sham-operated animals. WT and Sema4D−/− mice with ovariectomy and estrogen supplementation (OVX-E2) exhibit significant increases in uterine weight when compared with ovariectomized mice supplemented with oil (OVX-oil). Values shown are mean ± SEM. *$P<0.05$. OVX, ovariectomy; OVX-oil, ovariectomy plus oil supplementation; OVX-E2, ovariectomy plus 17β-estradiol supplementation.
(TIF)

Figure S2 The sites of Plexin-B1 cleaved by proprotein convertase. Plexin-B1, the Sema4D receptor, transforms from a precursor protein into an active protein via a conformational change that is caused by proprotein convertase-dependent cleavage of Plexin-B1. The proprotein convertase recognizes and cleaves the RXXR sequence residing in the target protein. A protein fragment presumed to result from the cleavage of R_{546}EERR and R_{1169}GPR of mouse Plexin-B1 is detected as a 75 kDa band on the western blot probed with anti-Plexin-B1 antibody (A-8). A-8 is a monoclonal antibody raised against the peptide fragment comprising amino acids 771-1070 of human plexin-B1, which is highly conserved with mouse plexin-B1 and covered by the 75 kDa region detected by western blot with A8. A previous study showed that the region covering the transmembrane and intracellular region, which is generated by proprotein convertase-mediated digestion of mouse plexin-B1, has a molecular size of 150 kDa [30]. EC: extracellular domain, TM: transmembrane domain, IC: intracellular domain, PCs: proprotein convertases.
(TIF)

Figure S3 Conversion of Sema4D and Plexin-B1 into respective soluble and active form during C57BL/6 vaginal development. The conversion of both Sema4D and Plexin-B1 into the respective soluble and active forms peaked 3.5 to 4 weeks (24 to 28 days) after birth; this time period does not coincide with the vaginal opening in C57BL/6 mice (37 days old).
(TIF)

Acknowledgments

We would like to thank all members of the Department of Physiology at Meijo University for their enthusiastic discussion and invaluable assistance.

Author Contributions

Conceived and designed the experiments: TI TT TK HK AK K. Yukawa. Performed the experiments: TI TB TT K. Yoshida TU TN. Analyzed the data: TI TB TT K. Yoshida TN K. Yukawa. Contributed reagents/materials/analysis tools: MM HT. Wrote the paper: TI K. Yukawa.

References

1. Rodriguez I, Araki K, Khatib K, Martinou JC, Vassalli P (1997) Mouse vaginal opening is an apoptosis-dependent process which can be prevented by overexpression of Bcl2. Dev. Biol. 184: 115–121.
2. Hübner A, Cavanagh-Kyros J, Rincon M, Flavell RA, Davis RJ (2010) Functional cooperation of the proapoptotic Bcl2 family proteins Bmf and Bim in vivo. Mol. Cell. Biol. 30: 98–105.
3. Lindsten T, Ross AJ, King A, Zong W-X, Rathmell JC, et al. (2000) The combined functions of proapoptotic Bcl-2 family members Bak and Bax are essential for normal development of multiple tissues. Mol. Cell 6: 1389–1399.
4. Simpson KJ, Wati MR, Deans AJ, Lindeman GJ, Brown MA (2004) MMTV-trBrca1 mice display strain-dependent abnormalities in vaginal development. Int. J. Dev. Biol. 48: 675–678.
5. Cano-Gauci DF, Song HH, Yang H, McKerlie C, Choo B, et al. (1999) Glypican-3-deficient mice exhibit developmental overgrowth and some of the

abnormalities typical of Simpson-Golabi-Behmel syndrome. J. Cell Biol. 146: 255–264.
6. Sundberg JP, Brown KS (1994) Imperforate vagina and mucometra in inbred laboratory mice. Laboratory Animal Science 44: 380–382.
7. Ito T, Bai T, Tanaka T, Yoshida K, Ueyama T, et al. (2014) Semaphorin 4D induces vaginal epithelial apoptosis to control mouse postnatal vaginal tissue remodeling. Mol Med Rep. in press.
8. Pasterkamp RJ (2012) Getting neural circuits into shape with semaphorins. Nat. Rev. Neurosci. 13: 605–618.
9. Kruger RP, Aurandt J, Guan KL (2005) Semaphorins command cells to move. Nat. Rev. Mol. Cell Biol. 6: 789–800.
10. Semaphorin Nomenclature Committee (1999) Unified nomenclature for the semaphorins/collapsins. Cell 97: 551–552.
11. Swiercz JM, Kuner R, Behrens J, Offermanns S (2002) Plexin-B1 directly interacts with PDZ-RhoGEF/LARG to regulate RhoA and growth cone morphology. Neuron 35: 51–63.
12. Nakamura F, Kalb RG, Strittmatter SM (2000) Molecular basis of semaphorin-mediated axon guidance. J. Neurobiol. 44: 219–229.
13. Janssen BJ, Robinson RA, Pérez-Branguli F, Bell CH, Mitchell KJ, et al. (2010) Structural basis of semaphorin-plexin signaling. Nature 467: 1118–1122.
14. Oinuma I, Ishikawa Y, Katoh H, Negishi M (2004) The semaphorin 4D receptor plexin-B1 is a GTPase activating protein for R-Ras. Science 305: 862–865.
15. Saito Y, Oinuma I, Fujimoto S, Negishi M (2009) Plexin-B1 is a GTPase activating protein for M-Ras, remodeling dendrite morphology. EMBO Rep. 10: 614–621.
16. Ito Y, Oinuma I, Katoh H, Kaibuchi K, Negishi M (2006) Sema4D/Plexin-B1 activates GSK-3β through R-Ras GAP activity, inducing growth cone collapse. EMBO Rep. 7: 704–709.
17. Basile JR, Afkhami T, Gutkind JS (2005) Semaphorin 4D/Plexin-B1 induces cell migration through the activation of PYK2, Src, and the phosphatidylinositol 3-kinase-Akt pathway. Mol. Cell. Biol. 25: 6889–6898.
18. Basile JR, Gavard J, Gutkind JS (2007) Plexin-B1 utilizes RhoA and Rho kinase to promote the integrin-dependent activation of Akt and ERK and endothelial cell motility. J. Biol. Chem. 282: 34888–34895.
19. Elhabazi A, Delaire S, Bensussan A, Boumsell L, Bismuth G (2001) Biological activity of soluble CD100. I. The extracellular region of CD100 is released from the surface of T lymphocytes by regulated proteolysis. J. Immunol. 166: 4341–4347.
20. Artigiani S, Barberis D, Fazzari P, Longati P, Angelini P, et al. (2003) Functional regulation of semaphorin receptors by proprotein convertases. J. Biol. Chem. 278: 10094–10101.
21. Shi W, Kumanogoh A, Watanabe C, Uchida J, Wang X, et al. (2000) The class IV semaphoring CD100 plays nonredundant roles in the immune system: defective B and T cell activation in CD100-deficient mice. Immunity 13: 633–642.
22. Li L, Tanaka T, Yukawa K, Akira S, Umesaki N (2009) Irinotecan-induced ovarian follicular apoptosis is attenuated by deleting the kinase domain of death-associated protein kinase. Int. J. Oncol. 34: 905–914.
23. Atwal JK, Singh KK, Tessier-Lavigne M, Miller FD, Kaplan DR (2003) Semaphorin 3F antagonizes neurotrophin-induced phosphatidylinositol 3-kinase and mitogen-activated protein kinase signaling: A mechanism for growth cone collapse. J. Neurosci. 23: 7602–7609.
24. Guan F, Villegas G, Teichman J, Mundel P, Tufro A (2006) Autocrine class 3 semaphorin system regulates slit diaphragm proteins and podocyte survival. Kidney Int. 69: 1564–1569.
25. Yamaguchi W, Tamai R, Kageura M, Furuyama T, Inagaki S (2012) Sema4D as an inhibitory regulator in oligodendrocyte development. Mol. Cell. Neurosci. 49: 290–299.
26. Moretti S, Procopio A, Lazzarini R, Rippo MR, Testa R, et al. (2008) Semaphorin3A signaling controls Fas (CD95)-mediated apoptosis by promoting Fas translocation into lipid rafts. Blood 111: 2290–2299.
27. Giacobini P, Messina A, Morello F, Ferraris N, Corso S, et al. (2008) Semaphorin 4D regulates gonadotropin hormone-releasing hormone-1 neuronal migration through PlexinB1-Met complex. J. Cell Biol. 183: 555–566.
28. Dacquin R, Domenget C, Kumanogoh A, Kikutani H, Jurdic P, et al. (2011) Control of bone marrow resorption by semaphorin 4D is dependent on ovarian function. PLoS ONE 6: e26627.
29. Hirschberg A, Deng S, Korostylev A, Paldy E, Costa MR, et al. (2010) Gene deletion mutants reveal a role for semaphorin receptors of the plexin-B family in mechanisms underlying corticogenesis. Mol. Cell. Biol. 30: 764–780.
30. Fazzari P, Penachioni J, Gianola S, Rossi F, Eickholt BJ, et al. (2007) Plexin-B1 plays a redundant role during mouse development and in tumour angiogenesis. BMC Dev. Biol. 7: 55.

Journal of Neuroimmunology 268 (2014) 43–49

Contents lists available at ScienceDirect

Journal of Neuroimmunology

journal homepage: www.elsevier.com/locate/jneuroim

Sema4A inhibits the therapeutic effect of IFN-β in EAE

Toru Koda [a,1], Tatsusada Okuno [a,*,1], Kazushiro Takata [a], Josephe Archie Honorat [a], Makoto Kinoshita [b], Satoru Tada [a], Masayuki Moriya [d], Saburo Sakoda [e], Hideki Mochizuki [a], Atsushi Kumanogoh [c], Yuji Nakatsuji [a,*]

[a] Department of Neurology, Osaka University Graduate School of Medicine, Suita, Osaka, Japan
[b] Department of Immune Regulation, Osaka University Graduate School of Medicine, Suita, Osaka, Japan
[c] Department of Respiratory Medicine, Allergy and Rheumatic Diseases, Osaka University Graduate School of Medicine, Suita, Osaka, Japan
[d] Department of Neurology, Toyonaka Municipal Hospital, Toyonaka, Osaka, Japan
[e] Department of Neurology, National Hospital Organization Toneyama National Hospital, Toyonaka, Osaka, Japan

ARTICLE INFO

Article history:
Received 12 September 2013
Received in revised form 12 December 2013
Accepted 31 December 2013

Keywords:
Multiple sclerosis (MS)
Experimental autoimmune encephalomyelitis (EAE)
Interferon-beta (IFN-β)
Sema4A

ABSTRACT

Approximately one-third of patients with multiple sclerosis (MS) respond poorly to interferon-beta (IFN-β) therapy. Serum Sema4A is increased in MS patients, and those who have high Sema4A do not respond to IFN-β therapy. In this study, we investigated whether recombinant Sema4A abrogates the efficacy of IFN-β in mice with experimental autoimmune encephalomyelitis (EAE), an animal model of MS. Administration of Sema4A concurrently with IFN-β diminished the efficacy of IFN-β in EAE. These effects of Sema4A were attributed to promote Th1 and Th17 differentiation and to increase adhesive activation of T cells to endothelial cells, even in the presence of IFN-β.

1. Introduction

Multiple Sclerosis (MS) is an inflammatory demyelinating disease of the central nervous system (CNS) that causes neurological disability in young adults (Noseworthy et al., 2000). Although several disease-modifying drugs (DMDs) have been developed (Ransohoff, 2007; Pelletier and Hafler, 2012; Sempere et al., 2013), interferon-beta (IFN-β) remains one of the most prescribed treatments for relapsing-remitting multiple sclerosis (RRMS). IFN-β therapy reduces overall relapse rates by approximately 30% and improves prognosis (Rudick and Goelz, 2011).

The mechanisms of action of IFN-β have been studied utilizing experimental autoimmune encephalomyelitis (EAE), an animal model of MS, along with assessment of clinical responses to IFN-β therapy in humans. The mechanisms of action of IFN-β involve multiple immunoregulatory functions, including blocking the trafficking of lymphocytes to the CNS (Floris et al., 2002), reducing expression of major histocompatibility class II molecules (Jiang et al., 1995), attenuating T cell proliferation and altering the cytokine milieu from pro-inflammatory to anti-inflammatory (McRae et al., 1998; Kozovska et al., 1999; Ramgolam et al., 2009).

Although IFN-β therapy is safe and generally well tolerated, a major problem with this therapy is that approximately one-third of patients with MS do not respond to the therapy (Rio et al., 2006). Because early initiation of appropriate treatments is necessary for a better prognosis (Kappos et al., 2007), distinguishing responders from non-responders prior to the initiation of treatment is critical. Although no established biomarkers exist that predict responsiveness to IFN-β, Th17-skewing are suggested to be related to IFN-β resistance (Lee et al., 2011; Balasa et al., 2013). We previously reported that high levels of serum Sema4A are correlated with nonresponsiveness to IFN-β therapy (Nakatsuji et al., 2012). However, the underlying mechanisms of how Sema4A affects the response to IFN-β remain unknown.

Sema4A is a membrane-type class IV semaphorin that we originally identified using a dendritic cell cDNA library (Kumanogoh et al., 2002). Although semaphorins were originally identified as axon guidance molecules that act during neural development, Sema4A also plays a crucial role in the immune and vascular systems (Kumanogoh et al., 2002, 2005; Toyofuku et al., 2007). In the immune system, Sema4A activates Th cells and promotes differentiation of Th1 and Th17 cells, whereas it is involved in angiogenesis and migration of endothelial cells by modulating vascular endothelial growth factor signaling in the vascular system (Toyofuku et al., 2007; Meda et al., 2012). Consistent with its important role in Th cells, Sema4A has been implicated in EAE. Treatment with anti-Sema4A antibodies inhibits antigen-specific T cell generation and ameliorates EAE (Kumanogoh et al., 2002). In addition, Sema4A is

* Corresponding authors at: Department of Neurology, Osaka University Graduate School of Medicine, D4, 2-2 Yamadaoka, Suita, Osaka 565-0871, Japan. Tel.: +81 6 6879 3571; fax: +81 6 6879 3579.
E-mail addresses: okuno@neurol.med.osaka-u.ac.jp (T. Okuno), yuji@neurol.med.osaka-u.ac.jp (Y. Nakatsuji).
[1] These authors contributed equally to this work.

0165-5728/$ – see front matter © 2014 Elsevier B.V. All rights reserved.
http://dx.doi.org/10.1016/j.jneuroim.2013.12.014

increased in the sera of patients with MS (Nakatsuji et al., 2012). These data together suggest that Sema4A plays critical roles in both MS and EAE.

In this study, we investigated whether recombinant Sema4A abrogates the efficacy of IFN-β in the EAE model of MS and analyzed the underlying mechanisms.

2. Materials and methods

2.1. Animals & reagents

Wild-type C57BL/6 female mice were purchased from Oriental Yeast Corp. (Tokyo, Japan) and were maintained in a specific pathogen-free environment. Experimental procedures were approved by the Animal Care and Use Committee of Osaka University Graduate School of Medicine (Permit Number: 20-084-6). All possible efforts were made to minimize animal suffering and limit the number of animals used. Recombinant murine IFN-β (PBL Biomedical Laboratories, Piscataway, NJ) and recombinant human IFN-β 1b (Bayer, Osaka, Japan) were used. Sema4A-Fc protein was made as previously described (Kumanogoh et al., 2002). Briefly, we generated recombinant soluble mouse Sema4A protein comprising the putative extracellular region fused to the human immunoglobulin 1 (IgG1) Fc fragment.

2.2. MOG-specific T cell response and cytokine assay

Eight to 11 weeks old C57BL/6 female mice were immunized with 100 μg myelin oligodendrocyte glycoprotein $(MOG)_{35-55}$ peptide (MEVGWYRSPFSPVVHLYRNGK) emulsified in complete Freund's adjuvant (CFA) containing 400 μg of *Mycobacterium tuberculosis* H37Ra (Difco Laboratories, MI, USA). For the recall assay, we collected the draining lymph nodes from mice 6 days after immunization. $CD4^+$ T cells were positively selected from the draining lymph nodes using an auto MACS cell purification system (Merck Millipore, Darmstadt, Germany), and 1×10^5 cells were restimulated for 72 hours with various concentrations of the MOG_{35-55} peptide in the presence of irradiated (3,000 rad) splenocytes (1×10^6 cells). Cytokines in the supernatant were assayed using mouse IFN-γ, IL-17A, IL-4 and IL-10 ELISA kits (R&D Systems, Minneapolis, MN, USA).

2.3. Induction of EAE and treatments

EAE was induced using a modification of our previously reported method (Takata et al., 2011). In brief, 8 to 11 weeks old C57BL/6 female mice were subcutaneously injected with 100 μg MOG_{35-55} emulsified in CFA supplemented with intraperitoneal injections of 200 ng pertussis toxin (List Laboratories, Campbell, CA, USA) on days 0 and 2.

For IFN-β treatment, IFN-β 1b (10,000 U) or phosphate buffered saline (PBS) was intraperitoneally injected to immunized mice every other day from days 0 to 10 after immunization. In addition, Sema4A-Fc (20 μg) or control human IgG (20 μg) was intravenously injected on days 0, 1, 3, 5, 7, 9 and 10 after immunization. All mice were monitored daily for clinical signs and were scored as follows using a scale of 0–5: 0, no overt signs of disease; 1, limp tail; 2, hind limb paralysis; 3, complete hind limb paralysis; 4, complete forelimb paralysis; 5, moribund state or death.

2.4. Histological and immunohistochemical analyses

Mice were sacrificed 22 days after immunization followed by transcardiac perfusion with 4% paraformaldehyde in PBS. For hematoxylin and eosin (H&E) staining, spinal cords were embedded in paraffin after perfusion with 4% PFA and 4 μm sections were cut from paraffin embedded blocks. Semi-quantitative histological analysis of inflammatory cellular infiltration was performed according to the following scoring system as previously described (Okuda et al., 2002): 0, no inflammation; 1, cellular infiltrates only in the perivascular areas and meninges; 2, mild cellular infiltration in the parenchyma; 3, moderate cellular infiltration in the parenchyma; 4, severe cellular infiltration in the parenchyma. For immunohistochemistry, Spinal cords were isolated, postfixed in 4% paraformaldehyde in PBS overnight, and then transferred to 30% sucrose in PBS overnight. Subsequently, the spinal cords were embedded in optimal cutting temperature (OCT) compound and frozen in liquid nitrogen. Frozen sections were cut at a thickness of 10 μm. For immunohistochemistry, the sections were incubated overnight at 4 °C with primary antibodies, followed by appropriate secondary antibodies for 2 hours at room temperature. The antibodies used in this study were as follows: rabbit anti-glial fibrillary acidic protein (GFAP) (1:500; Dako, Carpinteria, CA, USA), rabbit anti-Iba1 (1:500; Wako, Osaka, Japan), FITC-conjugated anti-CD3 (1:200; BD Biosciences, Franklin Lakes, NJ, USA), anti-von Willebrand factor (vWF) (1:500; Merck Millipore), anti-intercellular adhesion molecule (ICAM)-1 (1:50; BD Biosciences) and anti-vascular cell adhesion molecule (VCAM)-1 (1:50; Merck Millipore) antibodies. Images were captured by either a LSM510 laser scanning microscope (Zeiss, Thornwood, NY, USA) or a BZ9000 microscope (Keyence, Osaka, Japan). For quantification of T cells, microglia and astrocytes, we analyzed the density of CD3-, Iba1- or GFAP-positive cells, respectively, in every third sample section of horizontal spinal cord Sections. A total of 3 sections per mouse were analyzed and cell densities were counted in 4 randomly selected fields per section. We analyzed the area of double positive lesions of ICAM-1and vWF, and VCAM-1 and vWF in 4 randomly selected fields per section with NIS-elements software (Nikon, Tokyo, Japan). A total of 3 sections per mouse were analyzed.

2.5. Flow cytometry analysis

Lymphocytes were isolated from mice 6 days after immunization with MOG_{35-55}. Cells were washed twice with staining buffer containing 2% fetal bovine serum (FBS) and 0.09% sodium azide at pH 7.4 (BD Biosciences). To decrease non-specific cell staining, Fc receptors were blocked by incubating cells for 15 minutes on ice with an optimal concentration of rat anti-mouse CD16/CD32 antibody (1:50; BD Biosciences) diluted in staining buffer. Cells were then stained for 30 minutes on ice in the dark in the presence of APC-Cy7-labeled anti-CD4 antibody (1:100; BD Biosciences), followed by incubation with the following biotinylated anti-integrin antibodies: anti-α4, anti-αL, anti-β1 and anti-β2 (1:100; BD Biosciences). Thereafter, cells were washed twice with staining buffer and stained with FITC-conjugated streptavidin for 30 minutes. After staining, cells were washed twice with staining buffer, resuspended in staining buffer and passed through a Becton Dickinson FACS CANTO-2 ™ flow cytometer with Diva ™ software.

2.6. bEnd.3 cell culture and treatment

bEnd.3 cells, a murine brain cerebrovascular endothelial cell line, were maintained in DMEM (Wako) supplemented with 10% FBS and 100 U/mL penicillin/streptomycin (Invitrogen, Carlsbad, CA, USA). bEnd.3 cells were incubated at 37 °C in a humidified incubator with 5% CO_2 and 95% air. Cells were stimulated with human IgG (20 μg/ml), Sema4A-Fc (20 μg/ml), IFN-β (5 U/ml) + human IgG (20 μg/ml) or IFN-β (5 U/ml) + Sema4A-Fc (20 μg/ml) for 6 hours. After stimulation, mRNA was collected for RT-RCR.

2.7. Adhesion assay

The adhesion of $CD4^+$ T cells to bEnd.3 cells was examined under static conditions as previously described with minor modifications (De Clerck et al., 1994). Briefly, we collected the lymphocytes from mice immunized with MOG_{35-55} emulsified in CFA 6 days after immunization. Lymphocytes from MOG_{35-55}-immunized mice were restimulated with the MOG_{35-55} peptide (50 μg/ml) for 24 hours. After restimulation,

$CD4^+$ T cells were positively collected from lymphocytes using an auto MACS cell purification system. $CD4^+$ T cells were labeled with 0.5 mM 2′,7′-bis(carboxyethyl)-5,6 carboxyfluorescein acetomethylester (BCECF-AM) (DOJINDO, Tokyo, Japan) in RPMI-1640 medium containing 10% FBS at 37 °C for 45 minutes and subsequently washed with PBS. bEnd.3 cells in 96-well plates were incubated for 24 hours and then treated with IFN-β (5 U/ml), recombinant Sema4A-Fc (20 μg/ml) or both for further 24 hours. Then, bEnd.3 cells were further incubated with BCECF-AM-labeled $CD4^+$ T cells at 37 °C for 1 hour. Thereafter, nonadherent cells were removed by washing with PBS. Fluorescence intensity was measured by SH-9000Lab (Corona Electric, Ibaraki, Japan).

2.8. Quantitative RT-PCR

RNA was isolated from bEnd.3 cells or homogenized flash-frozen mouse spinal cords and purified using ISOGEN (Nippon Gene Co., Tokyo, Japan) according to the manufacturer's recommendations. cDNA was generated from 100 ng each RNA sample with an oligo dT primer and ReverTra Ace reverse transcriptase (Toyobo, Osaka, Japan) according to the manufacturer's recommendations.

Real-time RT–PCR was performed using the thermal cycler TaqMan 7900HT Fast Real-Time PCR System (Applied Biosystems, Carlsbad, CA, USA). Combined primers and probes were purchased from Applied Biosystems: Actb (Mm00607939_s1), Vcam1 (Mm01320970_m1), Icam1 (Mm00516023_m1), Ifng (Mm01168134_m1) and Il17a (Mm00439618_m1). PCR reactions were performed in triplicate in 20 μl using the Taq Man Universal PCR Master Mix (Applied Biosystems) and 1 μl cDNA. RT-PCR was carried out at 95 °C (10 minutes), followed by 40 cycles of 94 °C (1 minute), 56 °C (1 minute) and 72 °C (2 minutes). The relative expression levels of each mRNA were calculated using the ΔΔCt method and normalized to β-actin. Results are expressed relative to the control group.

2.9. Statistical analysis

EAE data, quantitative RT-PCR results and ELISA data are presented as means ± SEM. Statistical significance was determined with one-way ANOVA. p-values less than or equal to 0.05 were considered statistically significant.

3. Results

3.1. Sema4A promotes Th1 and Th17 differentiation in the presence of IFN-β

Induction of myelin-reactive Th1 and Th17 cells is the first crucial step for the initiation and progression of EAE and MS (Ishizu et al., 2005; Goverman, 2009). IFN-β suppresses the differentiation of these cells (Guo et al., 2008; Durelli et al., 2009; Zhang et al., 2011). To investigate the association between Sema4A and IFN-β in Th1 and Th17 differentiation, we first immunized C57BL/6 mice with MOG_{35-55} and treated them with recombinant Sema4A-Fc in the presence of IFN-β. $CD4^+$ T cells were collected from draining lymph nodes by positive selection, and the cytokines produced from MOG-reactive $CD4^+$ T cells following restimulation with MOG_{35-55} were examined. IFN-β treatment alone suppressed IFN-γ and IL-17 production (Fig. 1A and B), as described previously (Guo et al., 2008; Zhang et al., 2011). Sema4A alone did not change the production of IFN-γ and IL-17. However, Sema4A in addition to IFN-β reversed the suppression of these cytokines by IFN-β alone, and increased the production to the level of mice receiving control IgG (Fig. 1A, B). IL-4 was not detectable under any conditions (data not shown). The level of IL-10 was not altered by IFN-β and/or Sema4A (Fig. 1C). These data suggest that Sema4A promoted Th1 and Th17 differentiation in the presence of IFN-β.

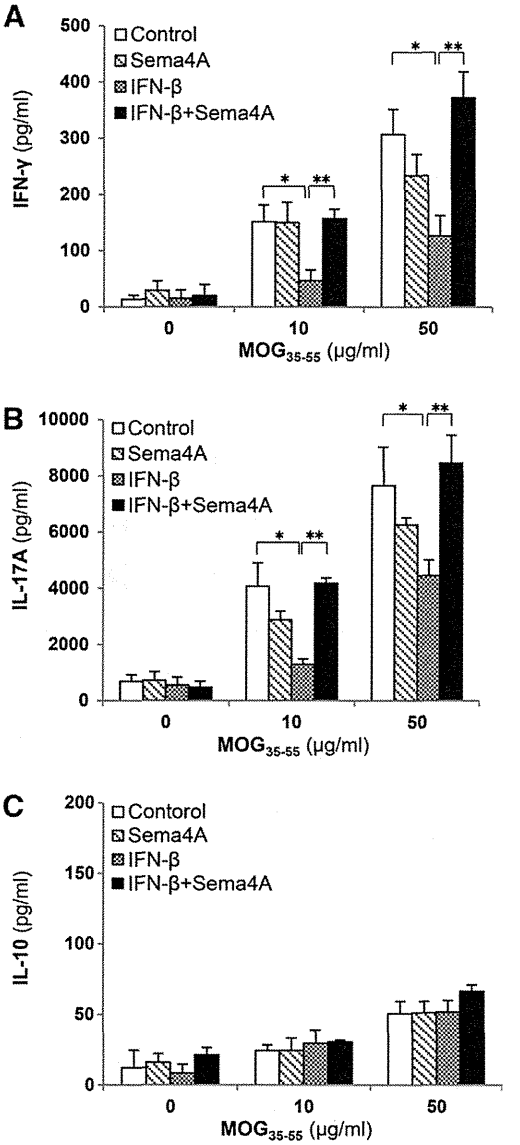

Fig. 1. Sema4A promotes Th1 and Th17 differentiation even in the presence of IFN-β. C57BL/6 mice were immunized with MOG_{35-55} and treated with PBS + human IgG (Control, n = 6), PBS + Sema4A-Fc (Sema4A, n = 6), IFN-β + human IgG (IFN-β, n = 6) or IFN-β + Sema4A-Fc (IFN-β + Sema4A, n = 6). Six days after immunization, $CD4^+$ T cells from the draining lymph nodes were restimulated for 72 hours with various concentrations of MOG_{35-55} in the presence of irradiated splenocytes from C57BL/6 mice. IFN-γ, IL-17 and IL-10 in the culture supernatants were assayed by ELISA. Data are the mean ± SEM of two independent experiments. $^*p \leq 0.05$; $^{**}p \leq 0.01$.

3.2. Sema4A promotes T cell adhesion to endothelial cells

After differentiation of encephalitogenic T cells, their adhesion to the endothelium is required for entry into the CNS and development of EAE and MS (Palmer, 2013). Very late antigen-4 (VLA-4, α4β1 integrin) and leukocyte function-associated antigen-1 (LFA-1, αLβ2 integrin) are needed for T cell tethering to the endothelium (Archelos et al., 1999). We examined whether the expression of VLA-4 and LFA-1 on $CD4^+$ T cells is increased by Sema4A. Recombinant Sema4A-Fc or IFN-β was administered to MOG_{35-55}-immunized C57BL/6 mice, and $CD4^+$ T cells were collected from draining lymph nodes to analyze the expression of VLA-4 and LFA-1. The expression levels of these integrins were not affected by Sema4A, IFN-β or a combination of these (Fig. 2A).

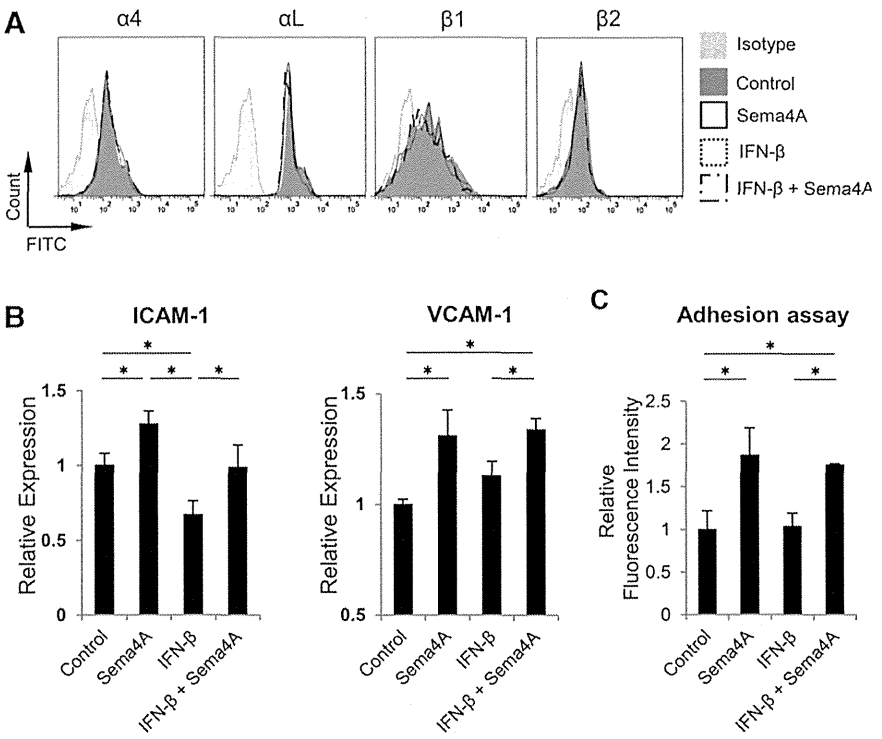

Fig. 2. Sema4A promotes T cell adhesion to endothelial cells. $CD4^+$ T cells were isolated from draining lymph nodes of MOG_{35-55}-immunized mice, which were treated with human IgG (Control), Sema4A-Fc (Sema4A), IFN-β + human IgG (IFN-β) or IFN-β + Sema4A-Fc (IFN-β + Sema4A) (n = 4 per each group). (A) α4, αL, β1 and β2 integrins on $CD4^+$ T cells were analyzed by flow cytometry. Sema4A did not affect the expression of LFA-1 or VLA-4. Data are representative of two independent experiments. (B) Relative mRNA expression of ICAM-1 and VCAM-1 in bEnd.3 cells. bEnd.3 cells were incubated for 1 day with human IgG (Control, n = 9), Sema4A–Fc (Sema4A, n = 9), IFN-β + human IgG (IFN-β, n = 7) or IFN-β + Sema4A-Fc (IFN-β + Sema4A, n = 7). Data are the mean ± SEM of four independent experiments. $^*p \leq 0.05$ (C) T cell adhesion to endothelial cells. bEnd.3 cells were stimulated with human IgG (Control, n = 3), Sema4A-Fc (Sema4A, n = 3), IFN-β + human IgG (IFN-β, n = 3) or IFN-β + Sema4A-Fc (IFN-β + Sema4A, n = 3). $CD4^+$ T cells were isolated from the spleens of MOG_{35-55}-immunized mice (n = 3). $CD4^+$ T cells were labeled with BCECF-AM and incubated on a bEnd.3 cell layer for 1 h. Then, nonadherent cells were removed, and the fluorescence intensity was measured. Sema4A promoted T cell adhesion to endothelial cells regardless of IFN-β treatment. Data are the mean ± SEM from a representative of three independent experiments. $^*p \leq 0.05$.

Next, we examined whether VCAM-1 and ICAM-1, ligands for VLA-4 and LFA-1, respectively that are expressed on endothelial cells, are affected by Sema4A with or without IFN-β. bEnd.3 cells were incubated with recombinant Sema4A-Fc in the presence or absence of IFN-β, and then the expression of mRNA for VCAM-1 and ICAM-1 was analyzed using quantitative RT-PCR. We found that Sema4A alone increased the expression level of ICAM-1 and VCAM-1 in endothelial cells (Fig. 2B). The enhanced expression of ICAM-1 and VCAM-1 by Sema4A was observed even in the presence of IFN-β. Consistent with RT-PCR analysis, immunohistochemical analysis also showed Sema4A enhanced the expression of ICAM-1 and VCAM-1 in bEnd.3 compared to those stimulated control IgG (Supplementary Fig. 1A and B). Furthermore, we performed an adhesion assay using splenic $CD4^+$ T cells and bEnd.3 cells in the presence of recombinant Sema4A-Fc and IFN-β. $CD4^+$ T cells were incubated with a cell layer of bEnd.3 cells that had been treated with Sema4A. Adhesion of T cells to the bEnd.3 cell layer was significantly increased compared to cells not treated with Sema4A (Fig. 2C). These results suggest that Sema4A promotes T cell adhesion to endothelial cells by increasing ICAM-1 and VCAM-1, even in the presence of IFN-β.

3.3. IFN-β is not effective in mice with EAE that received recombinant Sema4A-Fc

To determine whether Sema4A inhibits the beneficial effect of IFN-β in vivo, recombinant Sema4A-Fc was administered to mice with EAE that were also treated with IFN-β. IFN-β in the absence of Sema4A delayed the onset and attenuated the disease severity of EAE, as previously reported (Inoue et al., 2012). Although Sema4A alone did not affect the severity, administration of Sema4A concurrently with IFN-β resulted in exacerbation of EAE to a level similar to or worse than that in the control group (Fig. 3A).

Consistent with the clinical score, histological analysis with H&E staining of the spinal cord showed that mice receiving IFN-β exhibited reduced cellular infiltration, whereas Sema4A administration in addition to IFN-β increased cellular invasion compared to mice treated with IFN-β alone (Fig. 3B and C).

To further investigate the mechanism by which Sema4A abrogates the beneficial effect of IFN-β in EAE, spinal cord sections were stained with anti-CD3, -Iba1 and -GFAP antibodies to assess T cells, microglia and astrocytes, respectively. T cell infiltration and the activation of microglia and astrocytes were remarkably reduced in mice treated with IFN-β compared to control mice (Fig. 4A and B). Decreased cellular infiltration by IFN-β treatment was accompanied by a reduction in the mRNA expression of IFN-γ and IL-17 in the spinal cord (Fig. 4C). These results suggest that IFN-β ameliorates EAE by inhibiting Th1 and Th17 pathology. Administration of recombinant Sema4A alone did not significantly affect the mRNA expression of IFN-γ and IL-17, and no apparent differences in T cell infiltration or glial activation were observed compared to the control group. In contrast, when Sema4A was administered in addition to IFN-β, T cell infiltration and glial activation were apparently increased compared to mice receiving IFN-β alone (Fig. 4A and B). The decreased expression of IFN-γ and IL-17 mRNA by IFN-β was abrogated by additional administration of Sema4A (Fig. 4C). Consistent with mRNA levels of these cytokines, IFN-β alone decreased IFN-γ-positive cells and IL-17-positive cells in spinal cords, whereas Sema4A

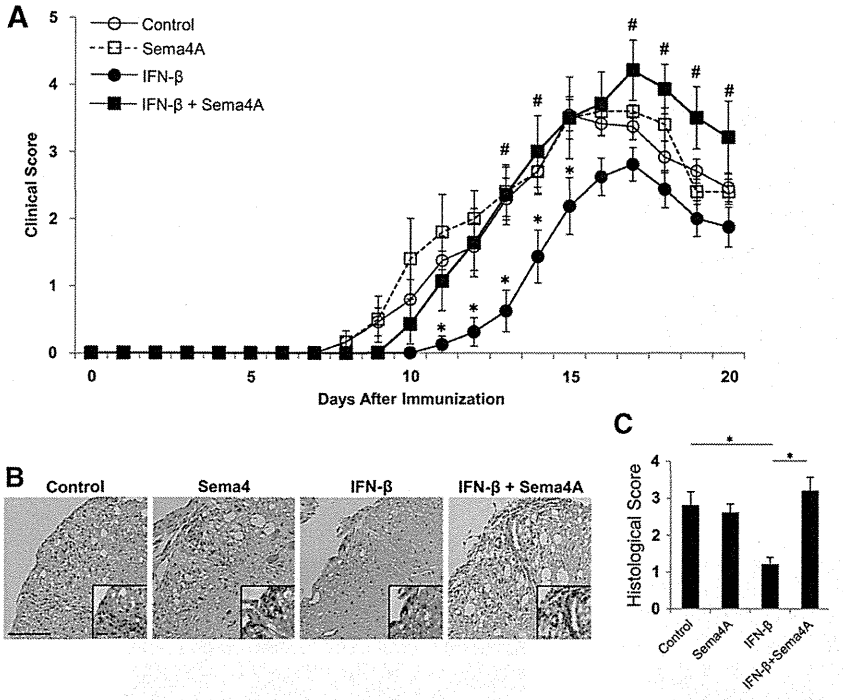

Fig. 3. Sema4A inhibits the efficacy of IFN-β in mice with EAE. (A) The mean clinical scores of mice with EAE are shown. Immunized mice were treated with PBS + human IgG (Control; open circles, n = 10), PBS + Sema4A-Fc (Sema4A; open squares, n = 8), IFN-β + human IgG (IFN-β; filled circles, n = 8) or IFN-β + Sema4A-Fc (IFN-β + Sema4A; filled squares, n = 8). Sema4A exacerbated the clinical score to the level of the control group, even in the presence of IFN-β. Data represent the mean score ± SEM of two independent experiments. $^{*}p \leq 0.05$ for IFN-β versus Control; $^{\#}p \leq 0.05$ for IFN-β + Sema4A versus IFN-β. Representative images of H&E staining of spinal cords on day 22 post-immunization (B) and the histological score (C) are shown. Sema4A promoted cellular infiltration in the presence of IFN-β. The insets in (B) show higher magnification of the spinal cords. Scale bars: 400 μm. Each bar in (C) indicates the mean pathological score ± SEM of three mice from each group. $^{*}p \leq 0.05$.

in addition to IFN-β increased infiltration of these cells to the level of control group (Supplementary Fig. 2A and B).

Because our in vitro data suggested that Sema4A promoted T cell adhesion to endothelial cells by increasing ICAM-1 and VCAM-1 expression, we next examined the expression of these adhesion molecules in the spinal cord of mice with EAE. The expression of VCAM-1 mRNA was significantly increased in mice treated with IFN-β plus Sema4A compared to mice treated with IFN-β alone. ICAM-1 expression also tended to increase following treatment with IFN-β plus Sema4A compared to mice treated with IFN-β alone (Fig. 4C), though the difference was not significant. Immunohistochemical analysis revealed that ICAM-1 and VCAM-1 were expressed on vWF-positive endothelial cells. Expression of ICAM-1 and VCAM-1 was increased in mice treated with IFN-β plus Sema4A compared to mice treated with IFN-β alone (Fig. 4D and E).

These data together suggest that Sema4A enhances not only Th1 and Th17 differentiation but also T cell adhesion to endothelial cells in the presence of IFN-β.

4. Discussion

In the current study, we investigated the implications of Sema4A on the efficacy of IFN-β by administering recombinant Sema4A-Fc and IFN-β to mice with EAE.

IFN-β confers its beneficial effect in MS and EAE through pleiotropic mechanisms of action. Among these, suppression of encephalitogenic T cells is one of the most important mechanisms. Reduction of T cell activation and proliferation, and induction of a shift toward anti-inflammatory cytokines have been shown to contribute to the efficacy of IFN-β (Kieseier, 2011). Concerning effector Th cell differentiation, IFN-β inhibits Th1 and Th17 differentiation (McRae et al., 1998; Durelli et al., 2009; Ramgolam et al., 2009). In contrast to the effects of IFN-β, Sema4A activates T cells and promotes Th1 and Th17 differentiation. Therefore, Sema4A may antagonize the suppressive effects of IFN-β on encephalitogenic T cells. Indeed, deterioration of EAE by Sema4A in the presence of IFN-β was accompanied by an increase in IFN-γ and IL-17 production by MOG-reactive Th cells as shown in Fig. 1.

We previously reported that the condition of MS patients with high Sema4A tends to deteriorate after IFN-β therapy. In the present study, recombinant Sema4A alone did not affect Th1 and Th17 reactions. However, Sema4A promoted the differentiation of these cells only when it was administered in combination with IFN-β. These data suggest that IFN-β may promote encephalitogenic T cell activation signaling downstream of Sema4A. IFN-β has not only anti-inflammatory but also pro-inflammatory effects including enhancing Th1 differentiation (Nagai et al., 2003) and increasing IL-6, an inflammatory cytokine that is required for development of Th17 cells (Ivanov et al., 2006; Nakatsuji et al., 2006; Kimura et al., 2007) under certain conditions. Indeed, patients with neuromyelitis optica, who are thought to have more IL-6 involvement than MS patients (Chihara et al., 2011), have been shown to deteriorate after receiving IFN-β therapy (Shimizu et al., 2010). Therefore, Sema4A may enhance IFN-β-induced pro-inflammatory reactions followed by increased pathogenicity of encephalitogenic T cells.

Th17 pathology has been implicated in the IFN-β resistance in MS (Axtell et al., 2010; Balasa et al., 2013). Axtell et al. reported that IFN-β exacerbates EAE induced by adoptive transfer of Th17 cells (Axtell et al., 2010) and suggested that IFN-β enhances Th17-mediated inflammation in the effector phase. Because MS patients with high Sema4A exhibit skewing towards Th17 condition, Sema4A and Th17 are thought to be closely linked in the context of IFN-β resistance. Indeed, we demonstrated that Sema4A promoted Th17 differentiation in the presence of IFN-β treatment. Therefore, exacerbation of EAE in the presence of

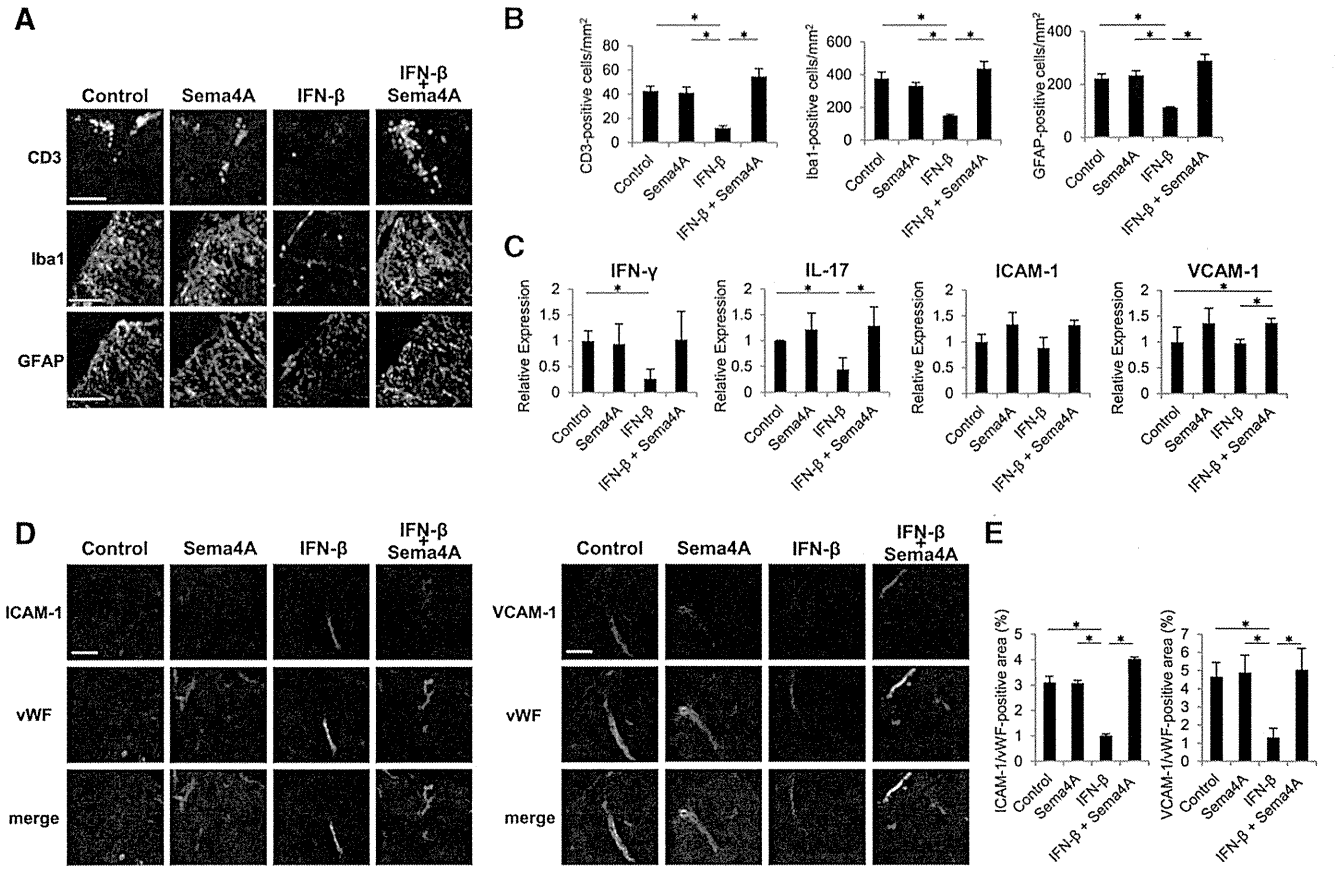

Fig. 4. Sema4A promotes T cell infiltration into the CNS and increases the expression of ICAM-1 and VCAM-1 in the CNS of mice with EAE. (A) Immunostaining with anti-CD3, -Iba1 and -GFAP antibodies in spinal cords of mice with EAE is shown. Mice with EAE were treated with PBS + human IgG (Control), PBS + Sema4A-Fc (Sema4A), IFN-β + human IgG (IFN-β) or IFN-β + Sema4A-Fc (IFN-β + Sema4A). Spinal cords were collected 22 days after immunization. Scale bars: anti-CD3; 100 μm, anti-Iba1; 50 μm, anti-GFAP; 50 μm. (B) The numbers of CD3-, Iba1- and GFAP-positive cells of spinal cord in each group are shown. Data presented in (A) and (B) is a representative of two animals. $^{*}p \leq 0.05$ (C) Expression of mRNA for IFN-γ, IL-17, ICAM-1 and VCAM-1 relative to that of mice with EAE treated with PBS + human IgG is shown (n = 4–5 per group). RNA was extracted from spinal cords of mice with EAE 21 days after immunization. Sema4A counteracted the inhibition of IFN-γ and IL-17 expression by IFN-β and promoted the expression of ICAM-1 and VCAM-1. Data are the mean ± SEM from a representative of two independent experiments. Double immunofluorescent staining with anti-ICAM-1/vWF and anti-VCAM-1/vWF in the spinal cord of mice with EAE (D) and quantitative analysis of immunohistochemical staining (E) are shown. Sema4A increased the expression of ICAM-1 and VCAM-1. Data presented in (D) and (E) is a representative of two animals. Scale bars: 50 μm. $^{*}p \leq 0.05$.

both Sema4A and IFN-β treatment may be partially due to enhanced Th17 differentiation by Sema4A.

In addition to the effect on encephalitogenic T cells, IFN-β has a profound effect on T cell migration into the CNS (Palmer, 2013). Of note, we found that Sema4A promoted T cell adhesion to endothelial cells by increasing the expression of ICAM-1 and VCAM-1 on endothelial cells. In this context, Sema4A may antagonize the efficacy of IFN-β, which limits lymphocyte migration across the blood–brain barrier. However, because Sema4A alone did not exacerbate the severity of EAE compared to controls, enhancement of T cell adhesion by Sema4A alone may not be sufficient to induce deterioration of EAE and MS. Sema4A-induced T cell adhesion may contribute to the pathogenesis of EAE and MS when combined with enhanced pathogenicity of encephalitogenic T cells.

Consistent with our previous study of patients with MS, Sema4A inhibited the therapeutic effect of IFN-β in mice with EAE. This abrogation was accompanied by an increase in antigen-specific Th1 and Th17 cell differentiation and T cell adhesion to endothelial cells. These results not only suggest a close link between Sema4A and IFN-β resistance but also support the notion that MS patients with high Sema4A will be non-responders to IFN-β therapy. Our findings imply that DMDs other than IFN-β may be appropriate for treatment of patients with MS who have high levels of Sema4A. Further investigation is required to select appropriate DMDs for MS patients with high Sema4A.

Supplementary data to this article can be found online at http://dx.doi.org/10.1016/j.jneuroim.2013.12.014.

Acknowledgments

This study was partly supported by the Health and Labor Sciences Research Grants for Research on Intractable Diseases from the Ministry of Health, Labor and Welfare of Japan.

References

Archelos, J.J., Previtali, S.C., Hartung, H.P., 1999. The role of integrins in immune-mediated diseases of the nervous system. Trends Neurosci. 22, 30–38.

Axtell, R.C., De Jong, B.A., Boniface, K., Van Der Voort, L.F., Bhat, R., De Sarno, P., Naves, R., Han, M., Zhong, F., Castellanos, J.G., Mair, R., Christakos, A., Kolkowitz, I., Katz, L., Killestein, J., Polman, C.H., De Waal Malefyt, R., Steinman, L., Raman, C., 2010. T helper type 1 and 17 cells determine efficacy of interferon-beta in multiple sclerosis and experimental encephalomyelitis. Nat. Med. 16, 406–412.

Balasa, R., Bajko, Z., Hutanu, A., 2013. Serum levels of IL-17A in patients with relapsing-remitting multiple sclerosis treated with interferon-beta. Mult. Scler. 19, 885–890.

Chihara, N., Aranami, T., Sato, W., Miyazaki, Y., Miyake, S., Okamoto, T., Ogawa, M., Toda, T., Yamamura, T., 2011. Interleukin 6 signaling promotes anti-aquaporin 4 autoantibody production from plasmablasts in neuromyelitis optica. Proc. Natl. Acad. Sci. U. S. A. 108, 3701–3706.

De Clerck, L.S., Bridts, C.H., Mertens, A.M., Moens, M.M., Stevens, W.J., 1994. Use of fluorescent dyes in the determination of adherence of human leucocytes to endothelial cells and the effect of fluorochromes on cellular function. J. Immunol. Methods 172, 115–124.